TU Delft

Delft University of Technology

Assessment of the Dynamic Properties of Holocene Peat

Zwanenburg, C.; Konstadinou, M.; Meijers, P.; Goudarzy, M.; König, D.; Dyvik, R.; Carlton, B.; Elk, J. Van; Doornhof, D.; Korff, M.

DOI
10.1061/(ASCE)GT.1943-5606.0002259

Publication date
2020

Document Version
Final published version

Published in
Journal of Geotechnical and Geoenvironmental Engineering

Citation (APA)
Zwanenburg, C., Konstadinou, M., Meijers, P., Goudarzy, M., König, D., Dyvik, R., Carlton, B., Elk, J. V., Doornhof, D., & Korff, M. (2020). Assessment of the Dynamic Properties of Holocene Peat. *Journal of Geotechnical and Geoenvironmental Engineering*, *146*(7), Article 04020049. https://doi.org/10.1061/(ASCE)GT.1943-5606.0002259

Important note
To cite this publication, please use the final published version (if applicable).
Please check the document version above.

Copyright
Other than for strictly personal use, it is not permitted to download, forward or distribute the text or part of it, without the consent of the author(s) and/or copyright holder(s), unless the work is under an open content license such as Creative Commons.

Takedown policy
Please contact us and provide details if you believe this document breaches copyrights.
We will remove access to the work immediately and investigate your claim.

This work is downloaded from Delft University of Technology.
For technical reasons the number of authors shown on this cover page is limited to a maximum of 10.

Assessment of the Dynamic Properties of Holocene Peat

C. Zwanenburg, Ph.D.[1]; M. Konstadinou, Ph.D.[2]; P. Meijers, Ph.D.[3]; M. Goudarzy, Ph.D.[4]; D. König, Ph.D.[5]; R. Dyvik, Ph.D.[6]; B. Carlton, Ph.D.[7]; J. van Elk[8]; D. Doornhof[9]; and M. Korff, Ph.D.[10]

Abstract: The dynamic behavior of a peat deposit in the north of the Netherlands is described. The organic content ranges from 70% to 95%, which is high compared to the organic content generally presented in publications on the dynamic behavior of peats. Shear wave velocities v_s and correspondingly small-strain shear moduli G_0 closely match values stated in the literature. Correlations stated in the literature for predicting G_0 proved to be applicable. Resonant column and cyclic direct simple shear tests were performed to establish the shear modulus reduction curves and damping curves. Excess pore pressure development during testing indicates dilatant behavior. The general trend shows nearly flat shear modulus reduction and damping curves at small strains regardless of organic content. Cyclic direct simple shear tests on humified material showed a larger pore pressure buildup than found in tests on non-to-moderately humified material. Differences in degree of humification did not result in significant differences in the shear modulus reduction curve, including G_0 values. Large scatter was found in the damping curves. For the humified material, tested at low stress level, a discontinuity in the damping curve is found at shear strain of 3%, which corresponds to a rapid pore pressure buildup in the tests. **DOI: 10.1061/(ASCE)GT.1943-5606.0002259.** *© 2020 American Society of Civil Engineers.*

Downloaded from ascelibrary.org by Technische Universiteit Delft on 05/13/20. Copyright ASCE. For personal use only; all rights reserved.

Introduction

The northeast part of the Netherlands, which primarily consists of the Dutch province of Groningen, is prone to earthquakes induced by gas production. Several risk assessment analyses have been conducted in order to estimate the consequences of future earthquakes. These include site response calculations to establish the amplification of the earthquakes in the shallow subsoil (Kruiver et al. 2017). Information about factors such as stiffness and damping is required for calculations of this kind. In the case of sands and clays, the relevant parameters can be obtained from well-established correlations in the literature. However, the area in question also includes peat deposits, the dynamic properties of which the literature provides limited information, which is summarized by Table 1.

With the aim of improving site response analysis for the Groningen area, a laboratory study was conducted to establish relevant dynamic properties of the main locally available peat deposit. This paper discusses the test results and the difficulty in establishing dynamic parameters for peat and compares the results with the data available from the literature. The aim of this paper is to generate more data for strong organic soils.

Research Strategy

The Groningen peat deposit consists of a surficial layer and a thin basal peat layer. The basal peat layer is too thin for sampling and was therefore not studied further. The thickness of the surficial peat layer ranges from 0 to, locally, 5 m. In general, the surficial peat layer is covered by a clay layer ranging in thickness from a few centimeters to 3 m. The effective overburden pressure is low at around 5 kN/m^2 where the top clay layer is practically absent or moderate and 25–30 kN/m^2 where the thickness of the top clay layer reaches 3 m. To cover the differences between low and moderate stress levels, samples with small and moderate overburden pressure were taken. The organic content levels reported in other studies are collected in Table 1. The values vary strongly and are generally lower than those found for the peat deposit tested in the present study.

The tested peat deposit includes patches of humified material. Landva (2007), for example, describes a strong influence of the fiber matrix on the static properties. There is no clear evidence that a fiber matrix also affects dynamic properties, but a possible effect was considered here by testing strongly humified and non-to-moderately humified peat samples. It should be noted that, in strongly humified peats, decay reaches a level at which fibers are no longer visually recognizable. Moreover, Landva (2007), Den Haan and Kruse (2007), and Cola and Cortellazzo (2005) have elaborated on the hypothesis that the fiber matrix is the main cause

[1]Geo-engineering, Deltares, P.O. Box 177, Boussinesqweg 1, 2629 HV, Delft 2600 MH, Netherlands; Delft Univ. of Technology, Delft, Netherlands (corresponding author). ORCID: https://orcid.org/0000-0002-8493-6943. Email: cor.zwanenburg@deltares.nl

[2]Geo-engineering, Deltares, P.O. Box 177, Boussinesqweg 1, 2629 HV, Delft 2600 MH, Netherlands. Email: maria.konstadinou@deltares.nl

[3]Geo-engineering, Deltares, P.O. Box 177, Boussinesqweg 1, 2629 HV, Delft 2600 MH, Netherlands. Email: piet.meijers@deltares.nl

[4]Chair of Foundation Engineering, Soil and Rock Mechanics, Ruhr Universität Bochum, P.O. Box 102148, Universitätsstrasse 150, Bochum D-44801, Germany. Email: meisam.goudarzyakhore@rub.de

[5]Chair of Foundation Engineering, Soil and Rock Mechanics, Ruhr Universität Bochum, P.O. Box 102148, Universitätsstrasse 150, Bochum D-44801, Germany. Email: diethard.koenig@rub.de

[6]Norwegian Geotechnical Institute, P.O. Box 3930, Sognsvn. 72, Oslo N-0855, Norway. Email: Rune.Dyvik@ngi.no

[7]Norwegian Geotechnical Institute, P.O. Box 3930, Sognsvn. 72, Oslo N-0855, Norway. Email: Brian.Carlton@ngi.no

[8]Shell, Industrieweg 46A, Assen 9403 AB, Netherlands. Email: Jan.Van-Elk@shell.com

[9]Shell, Industrieweg 46A, Assen 9403 AB, Netherlands. Email: dirk.doornhof@shell.com

[10]Geo-engineering, Deltares, P.O. Box 177, Boussinesqweg 1, 2629 HV, Delft 2600 MH, Netherlands; Delft Univ. of Technology, Delft, Netherlands. ORCID: https://orcid.org/0000-0003-1922-9609. Email: mandy.korff@deltares.nl

Note. This manuscript was submitted on April 12, 2018; approved on January 8, 2020; published online on April 23, 2020. Discussion period open until September 23, 2020; separate discussions must be submitted for individual papers. This paper is part of the ***Journal of Geotechnical and Geoenvironmental Engineering***, © ASCE, ISSN 1090-0241.

Table 1. Summary of literature data

Source	Location	σ_c' (kN/m^2)	OC (%)	ρ (Mg/m^3)	Type of test
Kramer (1996, 2000)	Mercer Slough, Washington	1.5, 12.5, 19	72.6–80.3	1.00–1.04	RC and CTX
Boulanger et al. (1998)	Sherman Island, California	66–200	44–65	1.13–1.20	CTX
Stokoe and Santamarina (2000)	Queensboro, New York	114	35–65	Not specified	RC and TS
Wehling et al. (2003)[a]	Sherman Island, California	12–78	21–52	1.06–1.24	CTX
Kishida et al. (2009a)	Montezuma Slough, California	17–67	15–61	1.06–1.33	CTX
Kishida et al. (2009a)	Clifton Court, New Jersey	55–220	14–35	1.20–1.46	RC and CTX
Tokimatsu and Sekiguchi (2006)	Ojiya, Japan	29/39	Not specified	Not specified	TS
Kallioglou et al. (2008)	Greece	370–400	48–62	1.32–1.43	RC
Shafiee (2016)	Sherman Island, California	12–100	10–70	1.0–1.6	cyDSS

Note: RC = resonant column test; TS = torsional shear; CTX = cyclic triaxial test; cyDSS = cyclic direct simple shear; σ_c' = applied consolidation stress; OC = organic content; and ρ = bulk density.
[a]Wehling et al. (2003) includes the tests presented by Boulanger et al. (1998) and gives additional tests.

Downloaded from ascelibrary.org by Technische Universiteit Delft on 05/13/20. Copyright ASCE. For personal use only; all rights reserved.

of the anisotropic behavior of peat. The absence of a fiber matrix due to humification should, in the light of this hypothesis, result in more isotropic behavior.

The laboratory testing consisted of 26 resonant column (RC) tests to determine the small-strain parameters. A total of 10 cyclic direct simple shear (cyDSS) tests were conducted to establish the medium- and large-strain behaviors. A series of 20 constant rate of strain (CRS) tests were used to establish the in situ yield stress σ_{vy}'. A series of 20 static direct simple shear tests (DSS) were conducted for the purposes of comparison with cyDSS results. Bender element tests were conducted on the specimens used for RC testing. The water content w, bulk density ρ, dry density ρ_{dry}, solid density ρ_s, and loss on ignition LOI were determined for each specimen tested. This set of parameters—w, ρ, ρ_{dry}, ρ_s, and LOI—is referred to as the classification parameters in the this paper. Samples were preferably taken in such a way that they could be split into a specimen for RC testing, a specimen for cyDSS testing, a specimen for CRS testing, and a specimen for static DSS testing. Unfortunately, layer thickness, sample sizes, and the heterogeneity of the peat deposit made it impossible to obtain complete sets for all the samples.

The study focuses on the behavior of the peat deposit in the field. The laboratory tests were therefore conducted at the field stress level and no other stress conditions were applied. To facilitate the assessment of field stresses, clay layers placed on top of the peat deposit were sampled, when relevant, to determine the unit weight and layer thickness.

Sample Location, Characterization of the Tested Material by CRS, and Static DSS Test Results

The sample location was selected on the basis of general geological knowledge of peat deposits in the Groningen area, archive information, and additional hand auger drillings to check the actual layer thickness and peat type. The three sample locations that were finally selected are shown in Fig. 1: Nieuwolda, Schildmeer, and Siddeburen. The distance between the locations was 5–10 km. All samples were taken from the surficial peat deposit that is geologically classified as the Nieuwkoop formation (Weerts et al. 2000). The patches of humified material are small and only a limited number of samples could therefore be taken from the humified material.

Sampling was conducted using a 100 mm piston sampler. The samples were visually inspected and classified by a geologist. The non-to-moderately humified peat found at the three locations consisted mainly of *Phragmites* (reed) and *Carex* (sedge). Inclusions of *Sphagnum* (sphagnum) and *Eriophorum* (cotton grass) were found at the Nieuwolda site. A few *Eriophorum* (cotton grass) inclusions were observed at the Schildmeer site. A botanical description of the strongly humified material cannot be given because plant remnants in the strongly humified material cannot be identified.

At the Siddeburen and Schildmeer sites, the subsoil consists of a clayey crust with a thickness of only 0.5 and 1.0 m, respectively, directly followed by the peat layer. At the Nieuwolda site the peat layer is situated below a 3-m-thick clay deposit, leading to larger stresses in the peat layer at this location. Annual fluctuations in the groundwater table result in a fluctuation in effective stresses. A 24-year record of groundwater measurements is available for the Nieuwolda and Siddeburen sites, and records going back 37 years are available for the Schildmeer location. The density of the top clay layer was determined with samples taken from the clay layer at the different testing locations. The vertical effective field stress levels were estimated for each of the tested specimens on the basis of the groundwater records and densities found for the clay and peat deposits. At the Nieuwolda site the vertical effective stress σ_v' ranges from 25 to 30 kN/m^2, from 6.5 to 10 kN/m^2 at Schildmeer, and from 5 to 7 kN/m^2 at Siddeburen.

The low vertical effective field stress levels observed at the Schildmeer and Siddeburen locations are typical for shallow peat deposits and are explained by the low density of peat in combination with a groundwater table close to ground level.

The one-dimensional stiffness characteristics and yield stress levels are obtained from CRS testing. The applied loading scheme consists of five steps: loading to 70 kN/m^2, followed by unloading to 14 kN/m^2, reloading to 140 kN/m^2, relaxation for 16 h, and reloading to 400 kN/m^2. The applied deformation rate is 0.3 mm/h, which corresponds to approximately 1.4%/h. Table 2 gives a summary of the obtained compression indices for normal compression CR and C_c, in which C_c is obtained from $C_c = CR(1 + e_0)$. Furthermore, Table 2 presents the ratios of CR/RR and C_α/CR, in which RR represents recompression index and C_α the creep parameter. The ratios of C_α/CR fit with values reported in literature; Mesri and Ajlouni (2007) report $C_\alpha/CR = 0.06 \pm 0.01$ for mainly North American peats, while Den Haan and Kruse (2007) report $0.07 < C_\alpha/CR < 0.125$ for Dutch peat deposits. Relations between compression index C_c and natural water content w_0 are reported by Hobbs (1986) ($C_c = 0.0065\, w_0$), Azzouz et al. (1976) ($C_c = 0.0115\, w_0$), and Mesri and Ajlouni (2007) ($C_c = 0.01\, w_0$). Fig. 2 shows the correlation for the three sample locations, $C_c = 0.0092\, w_0$, which corresponds nicely to the abovementioned relations. The scatter in C_c found for the Schildmeer location (Table 2) is perfectly explained by the correlation with w_0. The ratio CR/RR presented in Table 2 corresponds well to the values presented for Dutch peats by Den Haan and Kruse (2007).

Fig. 3 shows the overconsolidation ratio (OCR) values obtained from the test results. A fall in OCR was found at the Nieuwolda site, from OCR $= 1.6$ near the top of the peat deposit to 1.1 at lower depth.

Downloaded from ascelibrary.org by Technische Universiteit Delft on 05/13/20. Copyright ASCE. For personal use only; all rights reserved.

Fig. 1. Sample locations. (Map courtesy of Deltares.)

Table 2. Compression indices CR and C_c, unloading–reloading stiffness RR, and creep index C_α for the different sample locations; n represents the number of tests, and the presented ranges refer to the 95% upper and lower boundary values

Location	n	CR	C_c	CR/RR	C_α/CR
Nieuwolda	14	0.51 ± 0.02	5.03 ± 0.3	5.7 ± 0.4	0.08 ± 0.006
Siddeburen	2	0.44	4.07	12.2	0.12
Schildmeer	4	0.49 ± 0.05	5.6 ± 2.2	11.6 ± 1.1	0.10 ± 0.04

Note: The number of tests for the Siddeburen location is considered too small for statistical analysis.

A fall in OCR with depth is typical for many peat deposits in the Netherlands (Zwanenburg and Jardine 2015). Not enough CRS tests were conducted at Siddeburen and Schildmeer to establish a clear in-depth profile.

Figs. 4 and 5 show the in-depth profiles for water content w_0 and loss on ignition LOI. The water content is defined as the ratio of

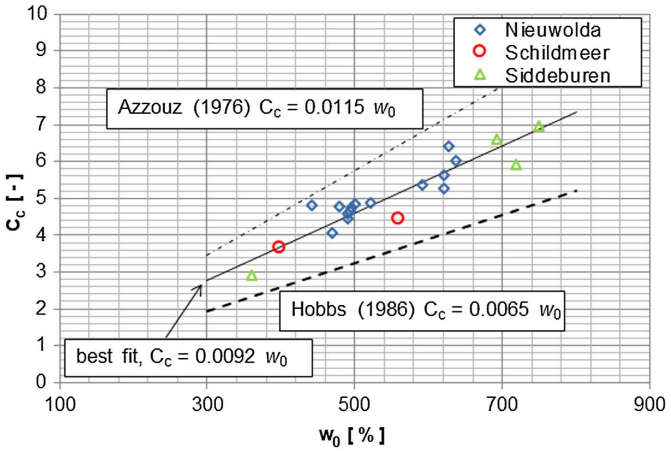

Fig. 2. Correlation between compression index C_c and natural water content w_0.

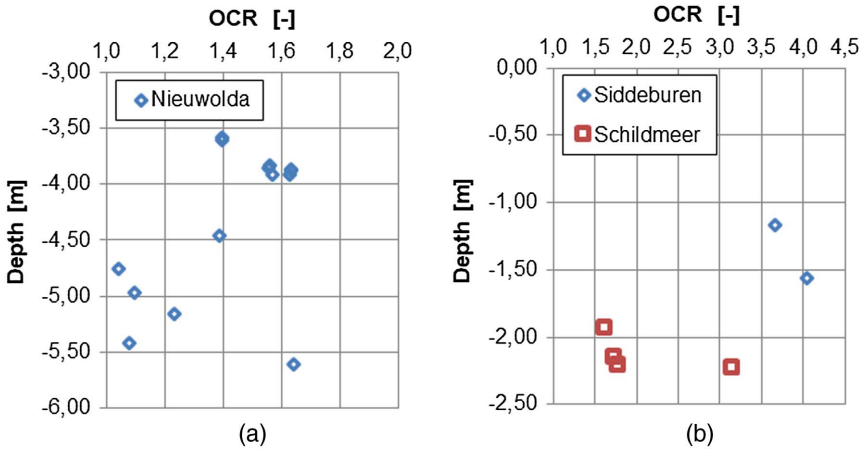

Fig. 3. Consolidation ratio *OCR* for (a) Nieuwolda; and (b) Schildmeer and Siddeburen, depth in meters below ground level.

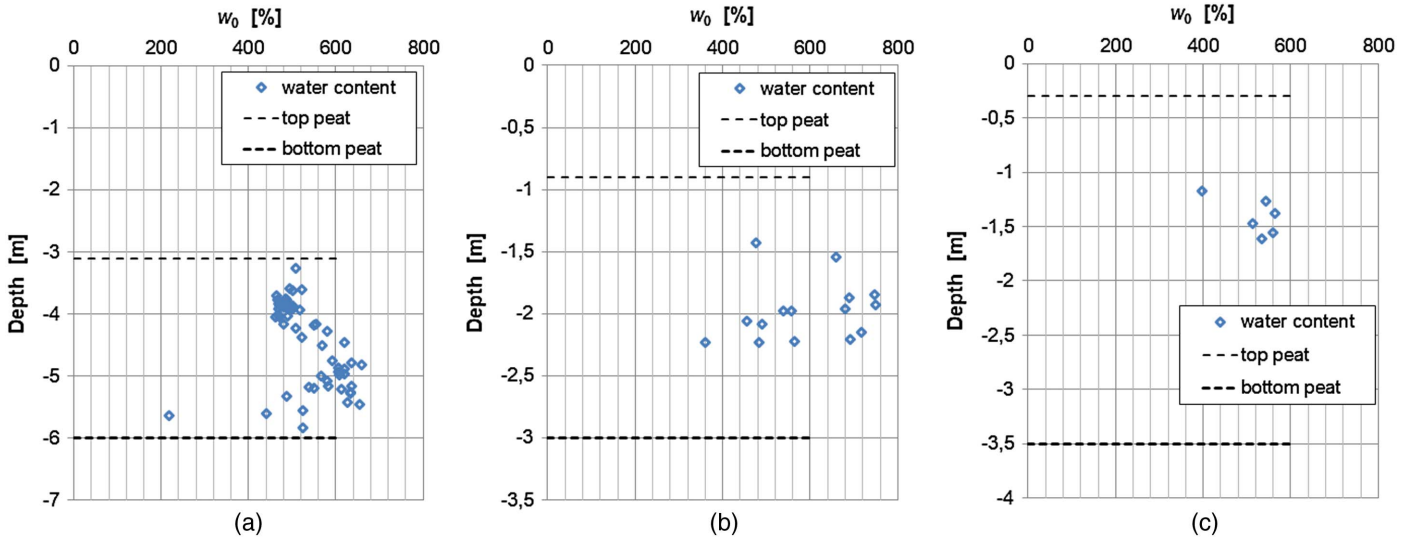

Fig. 4. Natural water content w_0 for (a) Nieuwolda; (b) Schildmeer; and (c) Siddeburen, depth in meters below ground level.

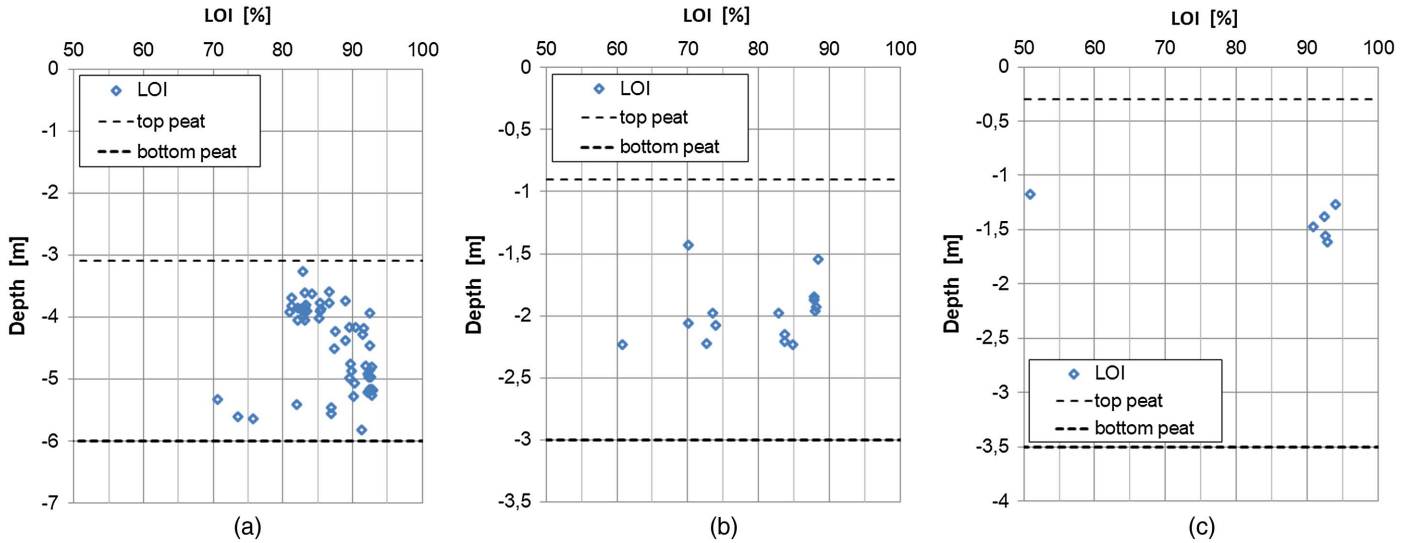

Fig. 5. Loss on ignition *LOI* for (a) Nieuwolda; (b) Schildmeer; and (c) Siddeburen, depth in meters below ground level.

J. Geotech. Geoenviron. Eng., 2020, 146(7): 04020049

Downloaded from ascelibrary.org by Technische Universiteit Delft on 05/13/20. Copyright ASCE. For personal use only; all rights reserved.

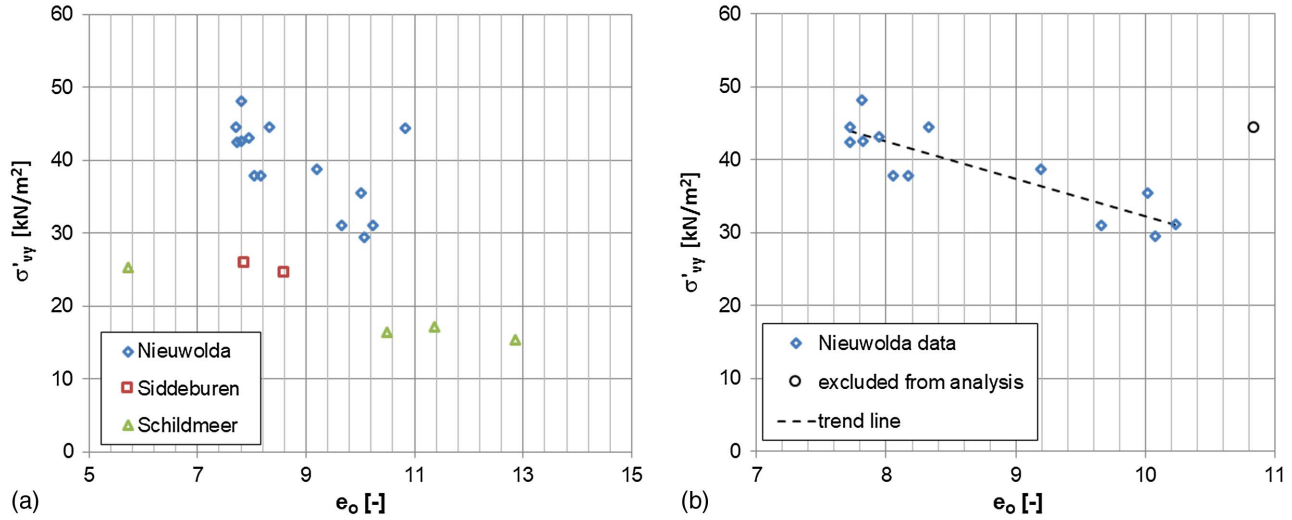

Fig. 6. Relation between initial void ratio e_0 and yield stress σ'_{vy} (a) for all CRS test data; and (b) for the Nieuwolda site; the circle indicates an outlying point which is excluded from the analysis.

water mass to solid mass and is determined for each specimen before testing. A range in w_0 between 360% and 748%, with a mean value of 556% for the non-to-moderately humified material is found and 485% for the humified material. The LOI is defined as the percentage of material lost when heating the sample. Different procedures are used by different researchers, ranging from 400°C over 12 h to 900°C over 1.5 h, Hobbs (1986). For temperatures above 450°C, present clay particles might lose fixed water or other nonorganic material. The OC is related to LOI by a correction factor C (Hobbs 1986)

$$OC = 100 - C(100 - LOI) \tag{1}$$

where OC and LOI are stated as percentages. For other temperatures, different values for C are required, ranging from 1.014 when heating to 400°C over 12 h to 1.168 when heating to 900°C over 1.5 h. Following Dutch standards (CROW 2015), a temperature of 550°C and burning time of 4 h is used in this study, resulting in $C = 1.04$ (Skempton and Petley 1970). The availability of different procedures might lead to small differences between OC values obtained by different researchers. The values for OC reported for tested samples in this publication are corrected using Eq. (1). The LOI of most samples ranged from 70% to 94%, with one value as low as 50.7% and an average value of 85.4 %. Using Eq. (1), OC was found to fluctuate between 68.8% and 93.8%, with an average value of 84.8%.

A correlation between w_0 and LOI is visualized by comparing Figs. 4(a) and 5(a), and an in-depth increase in both w_0 and LOI is found until 5–5.5 m below ground level. A reduction in both properties is found at a lower level. Also, for compressible materials such as peat, stress fluctuation in the past will influence the pore volume and hence water content. Comparison of Figs. 3(a) and 5(a) shows that the OCR profile mirrors the w_0 profile. OCR falls in depth between 3.5 and 5 m below ground level, while w_0 increases. The depth of the lowest OCR coincides with the depth of the largest w_0.

The initial dry density $\rho_{dry,i}$ is determined for each tested specimen by dividing the dry mass of the entire specimen after testing by the sample volume prior to testing. Also, the solid density ρ_s is determined from each specimen using a pycnometer following ISO (2015). This allows the determination of the initial void ratio $e_0 = (\rho_s/\rho_{dry,i}) - 1$ for each individual specimen. Fig. 6(a) shows the correlation between the initial void ratio e_0 and yield stress σ'_{vy} as obtained from the CRS test data. The combined data from all three locations results in a weak correlation, but there is a clear trend for the individual sites when the differences between humified and nonhumified material are considered, as shown in detail in Fig. 6(b) for nonhumified material in the Nieuwolda case.

Undrained shear strength parameters are obtained from static DSS tests. The samples are consolidated at field stress level and sheared at a rate of 8%/h at a constant height. For 10 tested specimens a CRS test was conducted on a specimen from the same sample. This allows relating the undrained shear strength s_u to OCR, following Ladd and Foot (1974):

$$s_u = S(OCR)^{\mu}\sigma'_v \tag{2}$$

in which S = undrained shear strength ratio for normally consolidated conditions; and μ = strength gain factor. Fig. 7 shows the results of fitting Eq. (2) to the peak strength values found in the DSS test, with $S = 0.58$ and $\mu = 0.76$ and a weighted least squares sum $R^2 = 0.85$. Values for S_{DSS} reported in literature for peats

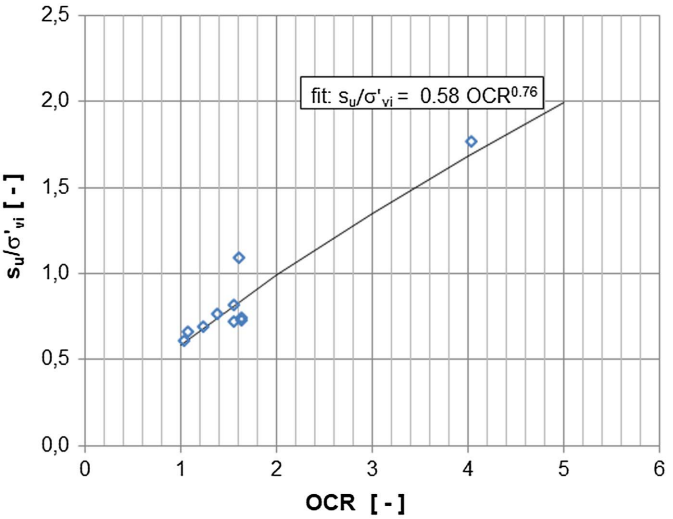

Fig. 7. Relation between normalized undrained shear strength s_u/σ_{vi} and OCR found from static DSS tests.

Downloaded from ascelibrary.org by Technische Universiteit Delft on 05/13/20. Copyright ASCE. For personal use only; all rights reserved.

are scarce. Mesri and Ajlouni (2007) provide a literature overview of the undrained shear stress ratio for a large range in peats based on triaxial testing S_{TX} and report $0.4 < S_{TX} < 0.8$. Zwanenburg and Jardine (2015) find $S_{DSS} = 0.47$ for Dutch peats, with w_0 ranging between 645% and 1,240% and LOI between 75 and 95%.

Wroth (1984) and others relate μ, Eq. (2), to the compression indices by $\mu = (CR–RR)/CR$. Applying this relation to the CRS test results yields $\mu = 0.85 \pm 0.02$ for all samples and 0.82 ± 0.01 for the Nieuwolda location, which is slightly larger than found in Fig. 7.

Humified and Nonhumified Samples Compared

Several researchers (Landva 2007; Cola and Cortellazzo 2005) indicate that the fibrous nature of peat has an influence on its mechanical behavior. The influence is reflected by anisotropy in stiffness and strength. For strongly humified peats the fiber structure at the macro level has decayed and is either weak or no longer present. Den Haan and Kruse (2007) show that humified peat acts more isotropic than nonhumified peats when air dried and explain this behavior by the macrofiber matrix which is no longer present in humified peats. The Groningen peat deposit contains relatively small patches of humified material. To be able to test a possible influence of humification on the dynamic properties of peat, the samples are classified in two categories: humified and non-to-moderately humified.

There are no clear parameters and procedures available for the unique definition of the degree of humification of peat samples. The available methods are based on visual observations, an example being the well-known Von Post classification as explained by, for example, Landva (2007). This method provides an indication of the degree of humification and the outcome is highly subjective. The samples classified as non-to-moderately humified correspond to the Von Post classifications H1–H7. Humified material corresponds to H8–H10. It should be noted that the plant structure is no longer recognizable beyond Von Post classification H7.

Humification destroys organic material and therefore degrades the (macro)fiber matrix, resulting in an increase in ρ_{dry} and a reduction in e_0 and LOI. Hobbs (1986) states that with increasing humification the water content falls. For nonhumified peats the volume of intracellular water usually exceeds the water volume in the free pores. The intracellular water is released during humification, explaining the reduction in water content. To check the outcome of the visual classification of humified and non-to-moderately humified samples, the classification parameters obtained were subjected to statistical analysis. The results are given in the appendix. The statistical analysis is based on the total number of specimens (76) tested in RC, CRS, DSS or cyDSS testing. Only 13 specimens were classified as humified material, four of which were used for RC testing and three for cyDSS testing.

The appendix shows the average and the 5% upper and lower values for each of the classification parameters for the humified and non-to-moderately humified samples. Clear differences were found in the upper and lower limits between the humified and non-to-moderately humified material, indicating differences in scatter, with the largest scatter being found for the humified material.

The results of the statistical tests (see appendix) show that the differences in classification parameters between the humified and non-to-moderately humified material are statistically significant. As is to be expected, ρ, ρ_{dry}, and ρ_s were higher for the humified material and w_0, e_0, and LOI were lower. The differences found in the classification parameters support the visual classification into humified and non-to-moderately humified material.

Small-Strain Shear Modulus G_0 and Shear Wave Velocity v_s from Bender Element Testing

Each of the specimens used for RC testing was subjected to bender element measurements to establish the shear wave velocity v_s and the initial shear modulus G_0 using

$$G_0 = \rho \times v_s^2 \tag{3}$$

where ρ = bulk density of the tested sample.

The shear wave velocity v_s for all the RC samples was in the 20.3–40.6 m/s range, yielding a small-strain shear modulus G_0 ranging from 421 to 1,704 kN/m^2. All samples were tested at field stress level. However, as explained in the "Sample Location, Characterization of the Tested Material by CRS and Static DSS Test Results" section, the field stress level varied for the different sample locations. Testing of samples at σ'_v in the range of 7.6–13.3 kN/m^2 resulted in $v_{s,\text{ave}} = 31.6$ m/s and a coefficient of variation $COV = 0.14$, leading to $G_{0,ave} = 1{,}058$ kN/m^2 with $COV = 0.27$. The samples tested at σ'_v in the range of 25.3–27.7 kN/m^2 give $v_{s,ave} = 34.2$ m/s with $COV = 0.14$, yielding $G_{0,ave} = 1{,}244$ kN/m^2 with $COV = 0.26$. The coefficient of variation for v_s is smaller than for G_0. This is in line with Eq. (3).

Fig. 8 shows shear wave velocity versus initial void ratio e_0, water content w_0, yield stress σ'_{vy}, and loss on ignition LOI. The graphs show no clear correlation between v_s and w_0 [Fig. 8(b)]. In addition, v_s does not seem to correlate with LOI [Fig. 8(d)]. However, the range for LOI in the tested samples is small. Fig. 8(c) shows the relation between v_s and σ'_{vy}. Only the data points for which a CRS test was conducted on a specimen taken from the same sample are shown, resulting in fewer data points than shown in the other graphs.

Wehling et al. (2003) propose a relation between the normalized small-strain shear modulus G_0/p_a, in which p_a is the atmospheric pressure and σ'_v is the vertical effective stress level, by

$$\frac{G_0}{p_a} = A\left(\frac{\sigma'_v}{p_a}\right)^n OCR^m \tag{4}$$

and propose, based on tested samples from Sacramento–San Joaquin delta, for $w_0 = 236\%$–588% and $OC = 21\%$–65%, that $n = 0.87$, $m = 0.65$, and $A = 75.7$. Fig. 9(a) shows that Wehling et al. (2003) overpredicts the results obtained in this study. The differences might be explained by the differences in OC and applied stress levels. Kishida et al. (2006) relate A to OC by

$$A = \exp\left[5.2 + 0.48\frac{2}{1+\exp(OC/23)} + 0.74\left(\frac{3\frac{2}{1+\exp(OC/23)} - 1.5}{\ln\left\{1+3\exp\left[1+3\frac{2}{1+\exp(OC/23)}\right]\right\}} - 1\right)\right] \tag{5}$$

Kishida et al. (2006, 2009b) relate n and m to OC by

$$n = 1 - 0.37\frac{2}{1+\exp(OC/23)}, \quad m = 0.8 - 0.4\frac{2}{1+\exp(OC/23)} \tag{6}$$

Application of Eqs. (5) and (6) to the test data results in $0.966 < n < 0.987$, $0.763 < m < 0.786$, and $56.4 < A < 62.7$, in

Downloaded from ascelibrary.org by Technische Universiteit Delft on 05/13/20. Copyright ASCE. For personal use only; all rights reserved.

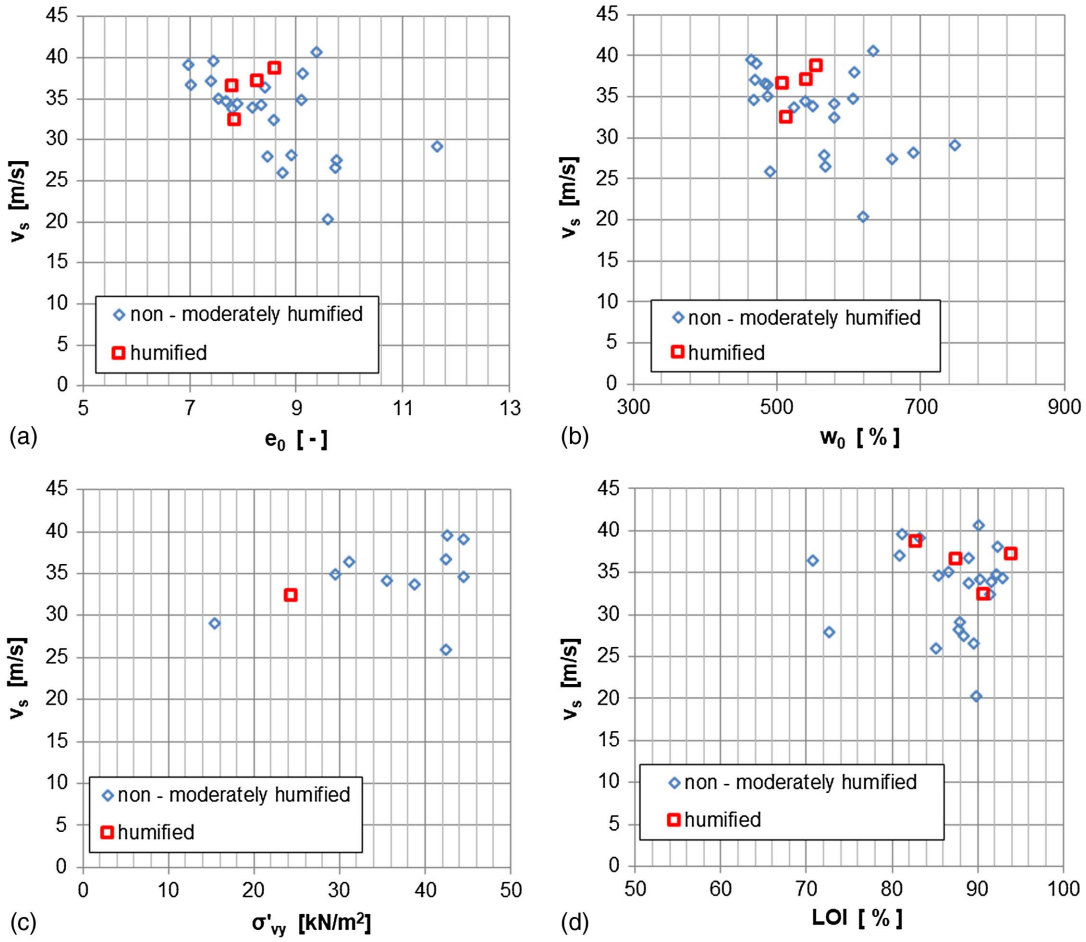

Fig. 8. Relation between shear wave velocity v_s: (a) initial void ratio e_0; (b) initial water content w_0; (c) yield stress σ'_{vy}; and (d) loss on ignition LOI.

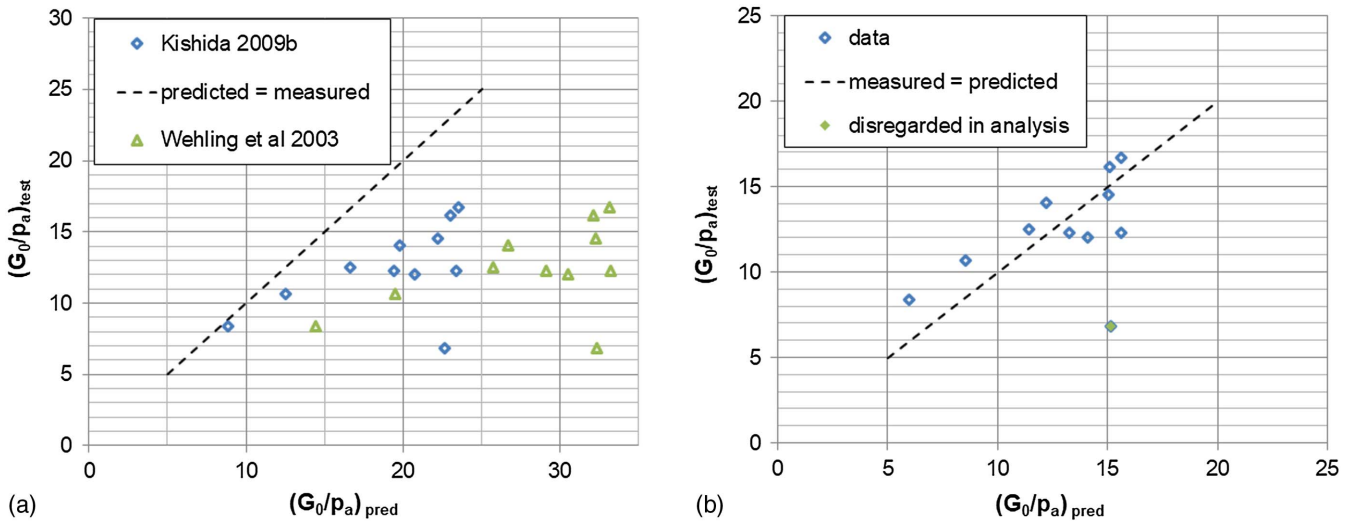

Fig. 9. Comparison between measured and predicted G_0/p_a: (a) using Eq. (4) (Wehling et al. 2003) and using Eqs. (5) and (6) from Kishida et al. (2006) and parameters from Wehling et al. (2003); and (b) using Eq. (6) and $A = 38.65$. Tests conducted for $OC = 69\%–92\%$ and $OCR = 1.08–1.84$.

which OC is determined on the basis of LOI in line with Eq. (1). The OC range for the tested samples is relatively small (69%–92%), and therefore the range for n, m, and A is small. Fig. 9(a) shows that using Eqs. (5) and (6) tends to improve the prediction of G_0/p_a compared to Wehling et al. (2003). It should be noted that Eqs. (5) and (6) were derived from tests on remolded peat with OC ranging from 16% to 81%. Alternatively, Fig. 9(b) shows the predicted values for Eq. (4), with n and m estimated by Eq. (6), and A is found by curve fitting, which results in $A = 38.65$.

Downloaded from ascelibrary.org by Technische Universiteit Delft on 05/13/20. Copyright ASCE. For personal use only; all rights reserved.

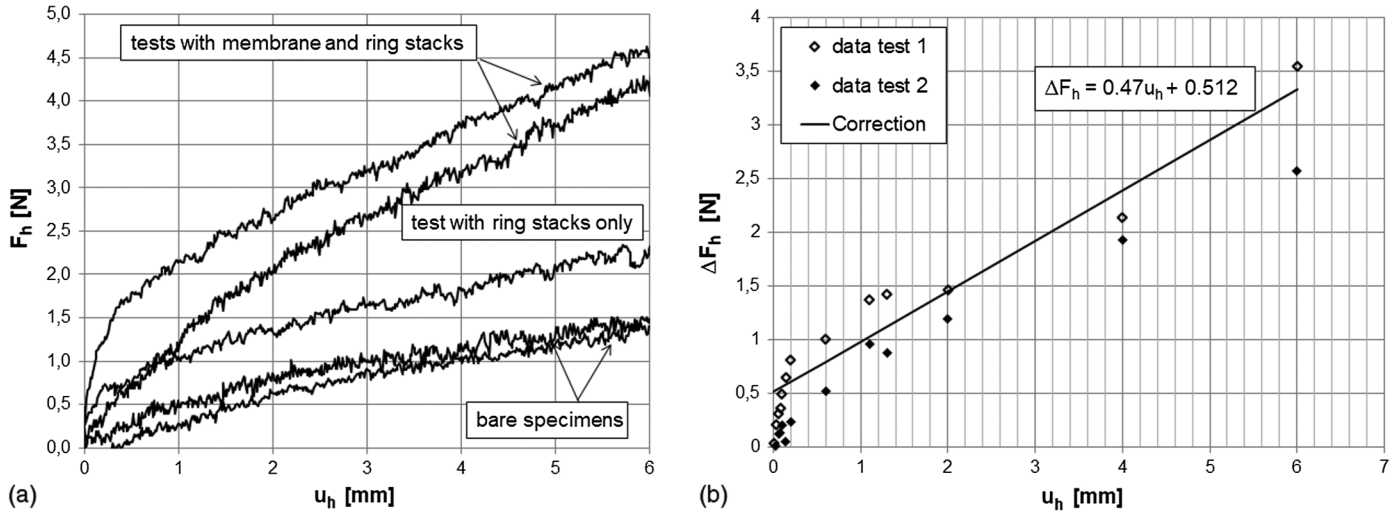

Fig. 10. Correction curve: (a) test results for bare and supported gelatine samples; and (b) applied correction curve. F_h represents horizontal force and u_h represents horizontal displacement.

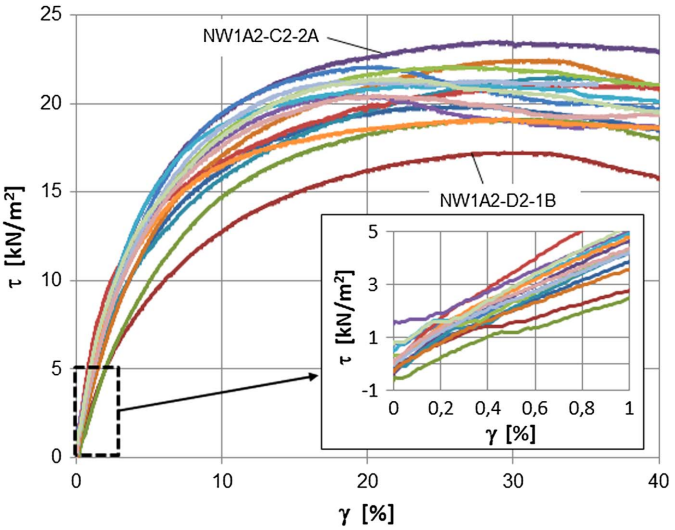

Fig. 11. Results of the static DSS tests on samples from the Nieuwolda site; stress–strain curves.

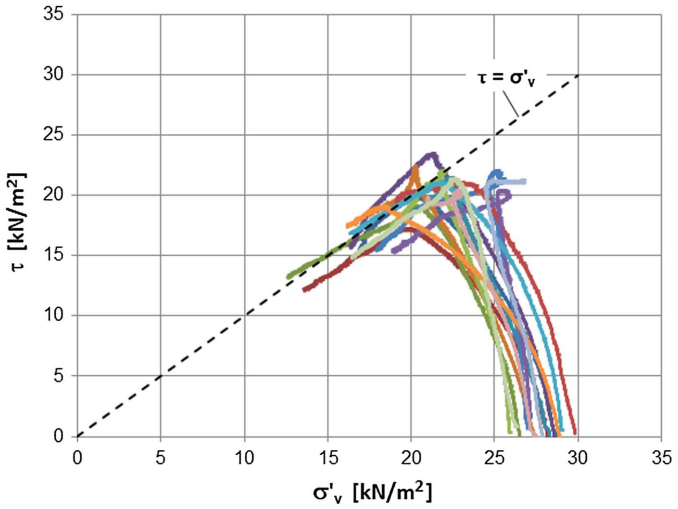

Fig. 12. Results of the static DSS tests on samples from the Nieuwolda site; shear stress paths, dotted line indicates $\tau = \sigma_v'$.

Cyclic and Static Direct Simple Shear Testing

Cyclic direct simple shear testing was conducted with Wille DSS equipment, part of the Wille Geotechnik series manufactured by APS (2019). A load cell with a maximum range of 500 N for vertical and horizontal loading was placed directly below the sample. For the sample dimensions used (diameter 63 mm, height 20 mm), the accuracies correspond to ± 0.03 kN/m^2 in the horizontal (shear) direction and ± 0.13 kN/m^2 in the vertical direction. The horizontal and vertical displacements were measured with LVDTs. A stack of rings with a membrane were used to support the sample. The sample height was actively controlled, while for cyclic testing the horizontal displacements were applied using a sinusoidal waveform.

Static DSS tests were conducted on gelatine specimens to derive a correction procedure for ring friction and membrane influence. These corrections are important when testing materials with very low shear strength. The gelatine specimens were produced by mixing gelatine powder (250 g/L) with glycerol (400 g/L) and water. Tests were conducted on a bare specimen, a specimen placed in the stack of rings, and a specimen placed in the stack of rings and membrane. The tests on the bare specimen and the specimen placed in the stack of rings and membrane were conducted in duplicate to determine reproducibility. Fig. 10(a) shows the results. The correction curve is found by comparing the measurement results for the specimen surrounded by rings and membrane to the bare sample. Fig. 10(b) shows the applied correction, which consists of a constant part that is explained by ring friction and a displacement dependent part that accounts for stretching the membrane.

To improve the understanding of the test results, a series of static DSS tests were conducted alongside the cyDSS tests. Figs. 11 and 12 show the results of 15 static DSS tests conducted on samples from the Nieuwolda site. Fig. 11 zooms in on the origin of the stress–strain curve and shows that, in most tests, the shearing phase starts with some initial shear stress. The initial shear stress is a result of the consolidation phase and develops directly when the vertical load is applied. This could be explained by inhomogeneity or anisotropy due to the fiber matrix of the sample, leading to a tendency for initial horizontal displacement, which was prevented during the consolidation phase.

Downloaded from ascelibrary.org by Technische Universiteit Delft on 05/13/20. Copyright ASCE. For personal use only; all rights reserved.

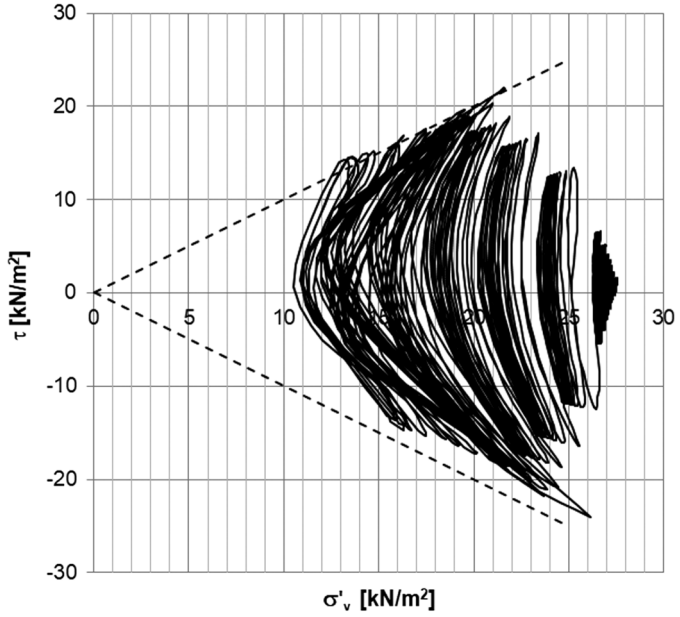

Fig. 13. Cyclic DSS test NW1A2-B1-2D result; shear stress path, dotted lines indicate $\tau = \sigma'_v$ and $-\tau = \sigma'_v$; $\sigma'_{vc} = 27.4$ kN/m^2.

Fig. 12 shows the shear stress paths. Height was constant in both the static and cyclic tests, and this is considered to be equivalent to undrained testing (Dyvik et al. 1987). Among others, Yamaguchi et al. (1985), Den Haan and Kruse (2007), and Zwanenburg and Jardine (2015) have shown that stress paths in triaxial testing with peat are bounded by the line $q/p' = 3$, in which q represents the deviator stress and p' the average of the three principal effective stresses. Den Haan (2014) has shown that this line is represented by $\tau = \sigma'_v$ in DSS tests on peat samples, when assuming that the stress conditions at failure in DSS testing are represented by the top of Mohr's circle. It should be noted that this assumption yields $\sigma'_v = \sigma'_h$ at failure. The dotted line in Fig. 12 shows $\tau = \sigma'_v$ and, as predicted by Den Haan (2014), the tests on the Nieuwolda samples tend to be bound by this line.

The "Shear Modulus Reduction Curve" and "Damping Curve" sections present a comparison of the cyDSS test results to the RC test results and bender element measurements. Some typical test results are discussed here. Figs. 13–17 show some results for test NW1A2-B1-2D. The tested specimen is a non-to-moderately humified specimen characterized by $w_i = 462.6\%$, $OC = 82.2\%$, and $e_0 = 8.0$. Cyclic displacement was applied at a frequency of 0.1 Hz and shear strain amplitudes ranging from 0.01 mm, $\gamma = 0.05\%$ to 6 mm, $\gamma = 30\%$. Ten cycles were applied per strain amplitude.

Fig. 13 shows a strong reduction in vertical stress found in the test. Similar to the static tests, Fig. 12, the shear stress paths seem to be bounded by the line $\tau = \sigma'_v$. Fig. 14(a) shows the stress–strain cycles observed in the test. The cycles for the larger applied shear strain γ_c clearly show degradation in mobilized shear strength τ with reducing maxima for cycles for a specific γ_c. Fig. 13 shows the reduction in vertical effective stress σ'_v during the test. The mobilized shear strain τ strongly depends on the vertical effective stress σ'_v, as visualized by normalizing the stress–strain curves by the actual vertical effective stress σ'_v, see Fig. 14(b). After normalization, the stress–strain cycles reduce to almost a single line. This shows that the changes in τ are explained by changes in σ'_v. Changes in σ'_v follow from the pore pressure changes, so the observed degradation in mobilized shear strain τ is mainly caused by pore pressure generation. It should be noted that in DSS testing the pore pressure is not measured directly. The tests are conducted under the constant volume condition, and change in vertical stress is interpreted as pore pressure development (Dyvik et al. 1987). The pore pressure increment Δu is related to the start of the shearing phase for the static tests and to the start of the cyclic loading for the cyclic DSS tests.

Fig. 15 shows a comparison of the cyDSS test NW1A2-B1-2D with the results of a static test on an adjacent specimen, test NW1A2-B1-2C. Fig. 15(a) compares the continuous, static, stress–strain curve with the maximum value τ_{max} for each cycle in the cyclic DSS test. Fig. 15(b) compares the shear modulus

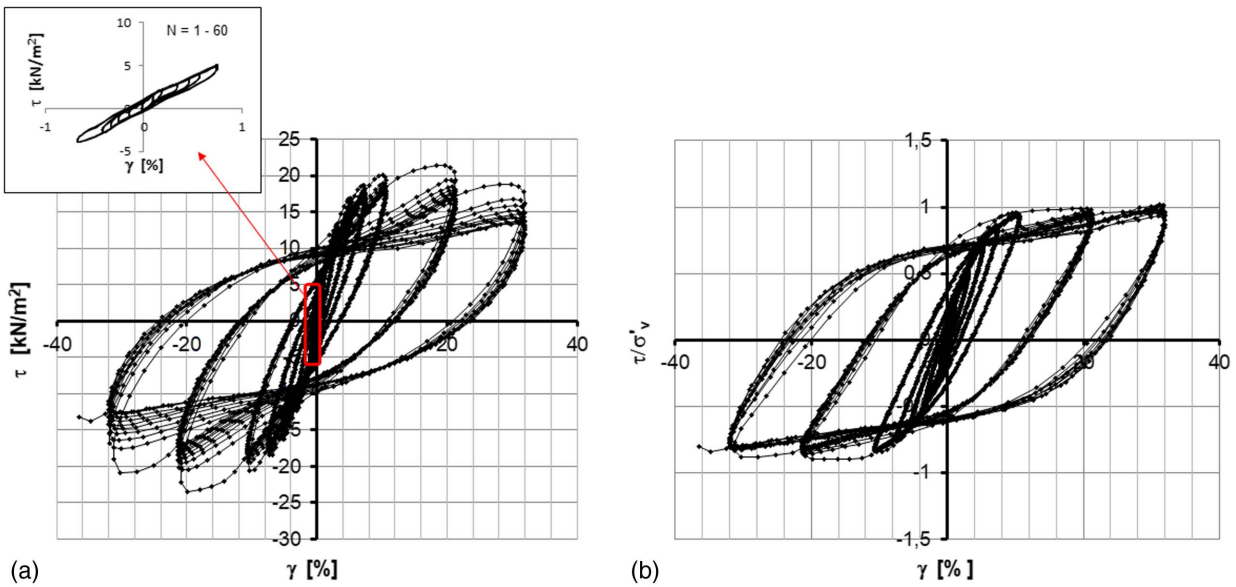

Fig. 14. Test results for cyclic DSS test NW1A2-B1-2D, $\sigma'_v = 27.4$ kN/m^2, $w_0 = 462.9\%$, $LOI = 82.2\%$: (a) shear stress versus shear strain; and (b) normalized shear stress versus shear strain.

J. Geotech. Geoenviron. Eng., 2020, 146(7): 04020049

Downloaded from ascelibrary.org by Technische Universiteit Delft on 05/13/20. Copyright ASCE. For personal use only; all rights reserved.

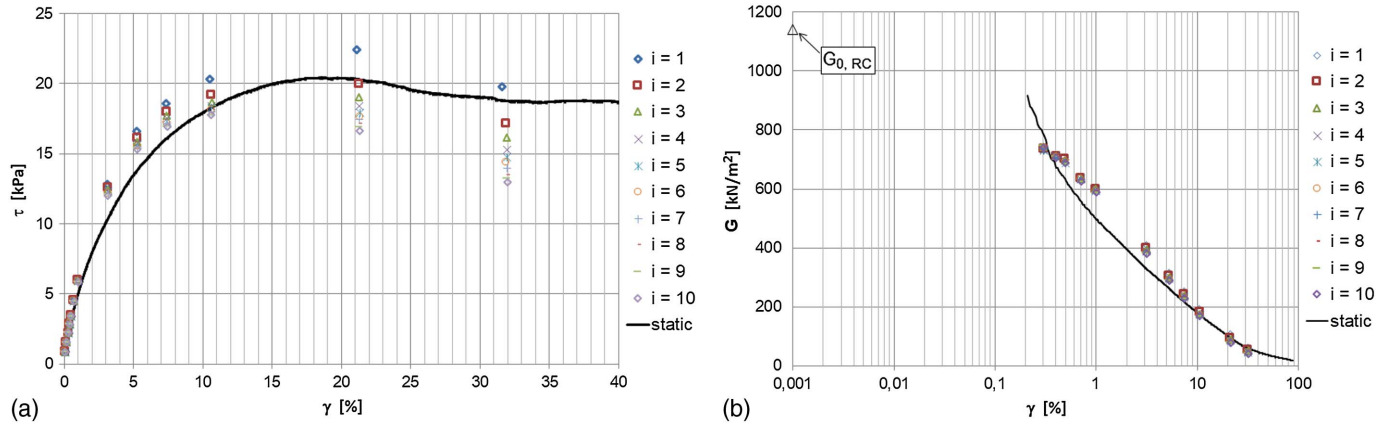

Fig. 15. Comparison of static and cyclic DSS tests, where i represents the cycle number for the different strain amplitudes: (a) stress–strain curve; and (b) shear modulus reduction curve.

degradation curve derived from the static and the cyclic tests. For a reference the G_{max} value found in the RC test on a specimen from the same sample is added. For strain amplitudes in the range of 0.5%–10%, behavior in the dynamic tests seems to be slightly stiffer than in the static tests. The differences can possibly be explained by rate effects. The applied monotonic strain rate $d\gamma/dt$ is 0.002%/s, while for the cyclic tests the strain rate increases from 0.002%/s for the smallest cycles to 3.18%/s for the largest cycles.

Fig. 15(a) also shows that degradation in shear strength of the sample becomes significant after exceeding the static peak strength; for example, in the case of $\gamma = 32\%$, $\tau_{max} = 19.81$ kN/m^2 in the first cycle and falls to 13.00 kN/m^2 in the tenth cycle. Despite the degradation of the sample at large strains, $\gamma_c > 10$, τ_{max} for the second cycle is in the same order of magnitude as τ_{static} at the equivalent strain level, despite the degradation in shear strength found in previous cycles. Apparently degradation in shear strength, or the amount of excess pore pressure, found at one strain level does not influence the initial shear strength found in the first cycle of the next tested strain level.

Following Idriss and Boulanger (2008), the excess pore pressure ratio r_u for cyDSS testing is defined as $r_u = \Delta u/\sigma'_{vc}$, in which Δu represents the excess pore pressure and σ'_{vc} the vertical consolidation stress prior to shearing. Fig. 16 shows the development of r_u for test NW1A2-B1-2D, which is a test on non-to-moderately humified material, and test NW1A2-A7-2C, which is the only Nieuwolda specimen that falls in the category of humified material. Cappa et al. (2017) report a 1% cyclic threshold shear strain beyond which Δu develops. Both specimens in Fig. 16 show a gradual increase at small-strain level with $r_u = 0.03$ respectively 0.1 at $\gamma_c = 1\%$ and a rapid rise in r_u for $\gamma_c > 1\%$. In these tests, and in the tests to be discussed later (Fig. 19), no clear threshold cyclic shear strain is observed. It should be noted that the humified specimen, NW1A2-A7-2C, reaches a larger r_u value compared to the non-to-moderately humified specimen NW1A2-B1-2D at the same γ_c level.

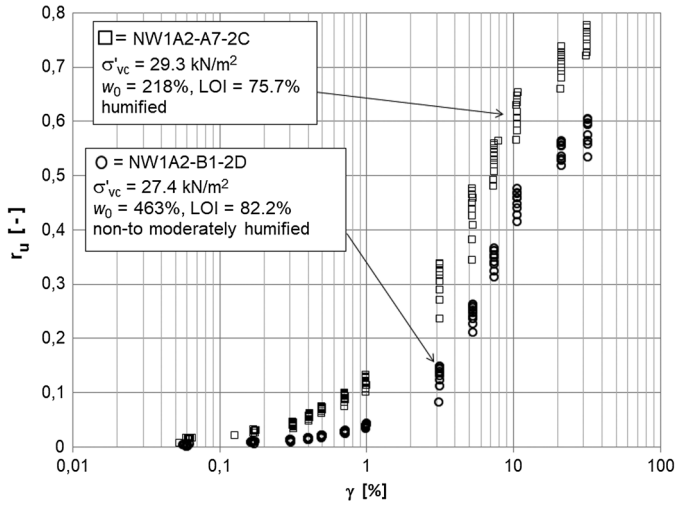

Fig. 16. Excess pore water pressure ratio r_u versus applied shear strain γ for non-to-moderately humified specimen NW1A2-B1-2D and humified specimen NW1A2-A7-2C.

The effect of cyclic degradation in shear modulus can be expressed by the degradation index δ described by Idriss et al. (1978):

$$\delta = \frac{G_1}{G_N} = N^{-t} \tag{7}$$

where G_1 represents the shear modulus in the first cycle, G_N the shear modulus in the Nth cycle, and N the cycle number. For purposes of comparison, the degradation parameter t was determined for $\gamma_c = 1\%$ for the tested material, with G_1 being determined on the basis of the first closed loop. It follows from test NW1A2-B1-2D that $t = 0.011$. Fig. 17 plots the t values for $\gamma_c = 1\%$ for all tests against the vertical consolidation stress σ'_{vc}. Basically, two groups of data points were found. One group comes from the tests for Schildmeer and Siddeburen. These tests were conducted at low stress levels. The second group consists of the Nieuwolda tests, which were conducted at moderate stress levels. The values are in the same range as those found by Wehling et al. (2003) at $\gamma = 1\%$.

In cyDSS testing, the damping ratio D per cycle is determined with

$$D = \frac{W_D}{4\pi W_S} \times 100\% \tag{8}$$

where W_D represents the energy dissipated in one cycle of loading and W_s the strain energy stored in one cycle. Fig. 18 shows the damping curve for test NW1A2-B1-2D. To show the influence of degradation on D for $\gamma_c = 32\%$, values for D are shown for cycles 1–10, which range from 24.7% to 28.3%.

Downloaded from ascelibrary.org by Technische Universiteit Delft on 05/13/20. Copyright ASCE. For personal use only; all rights reserved.

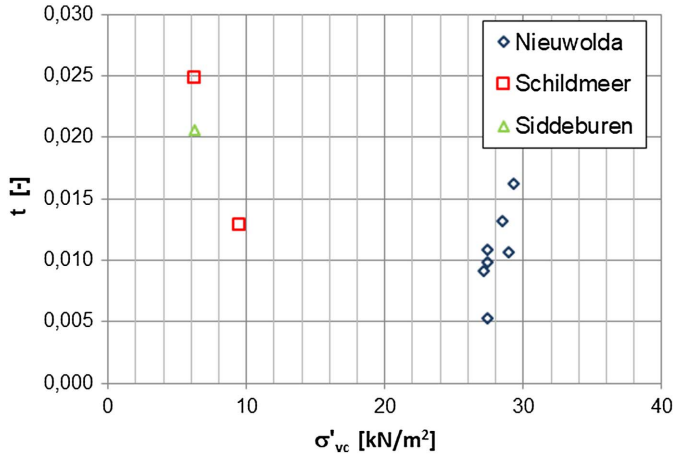

Fig. 17. Degradation parameters t at $\gamma = 1\%$. versus the vertical consolidation stress applied in the test σ'_{vc}.

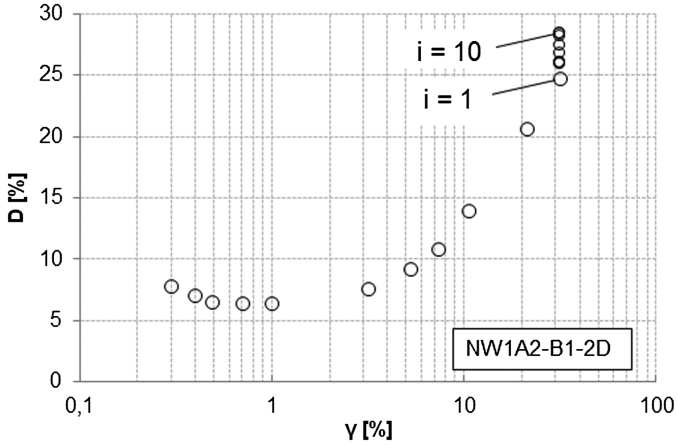

Fig. 18. Cyclic DSS test NW1A2-B1-2D, damping curve, damping ratio D, is determined for the second cycle. For $\gamma_c = 32\% D$ is presented for 1st–10th cycle with i = cycle number.

Regarding the damping curve, atypical behavior is found for the test from the Siddeburen, as shown by Fig. 19(a). Around $\gamma_c = 3\%$, a rapid increase in D is found, followed by a reduction for larger γ_c. To investigate this behavior, Fig. 19(b) compares the τ–γ cycles found for $\gamma_c = 1\%$ and 10%. For $\gamma_c = 1\%$, τ monotonically increases or decreases with increasing or decreasing γ. At $\gamma_c = 10\%$, however, only a small increase in τ is found between approximately $-5\% < \gamma < 5\%$. This behavior is further investigated by plotting the pore pressure development during the test [Fig. 19(c)]. Two phenomena can be observed in Fig. 19(c). The first phenomenon is the gradual pore pressure buildup during the successive cycles, with a clear increase in the initial cycles for $\gamma_c = 3\%$. A pore pressure buildup during undrained shearing reflects the tendency for compaction or volume reduction (Wood 1990). The second phenomenon is the strong pore pressure reduction at the end the cycles. Fig. 19(b) shows for the cycles at $\gamma_c = 10\%$ a small increase in τ and nearly constant r_u, Fig. 19(c), when $-5\% < \gamma < 5\%$ and a reduction in r_u for $\gamma > 5\%$ and $\gamma < 5\%$. De Groot et al. (2006) investigated liquefaction phenomena in cyclic tests on sand and found equivalent behavior when approaching sample failure, which is explained by dilative behavior. Fig. 19(c) shows that for relatively small γ_c the behavior is dominated by the tendency for compaction, shown by the pore pressure buildup during the successive cycles. For the larger γ_c values dilative behavior dominates. This is shown by the series for $\gamma_c = 10\%$ in Fig. 19(c), where the pore pressure buildup during the cycles is negligible and a strong, reversible pore pressure decrease is found for $\gamma = \pm\gamma_c$.

Fig. 19(d) shows the excess pore pressure ratio r_u. The value for r_u rises strongly for the successive cycles at $\gamma_c = 3\%$, which is explained by the increase in plastic deformation observed at $\gamma_c = 3\%$. In the following strain cycles r_u reaches 0.9. The shear modulus reduction curve, which will be discussed later in Fig. 23, shows a continuous curve around $\gamma_c = 3\%$, indicating that the sample did not fail completely. However, the behavior of the damping curve at $\gamma_c = 3\%$ and beyond is explained by the strong development of plasticity in the sample.

Test SB4A-A2-1C, discussed in Figs. 19(a–d), is classified as humified material. For the Schildmeer location two cyDSS tests have been conducted: test SMC2C-B1-2C, which is classified as non-to-moderately humified material, and SM2C-A3-1C, which is classified as humified material. Fig. 19(e) shows the r_u development found in both tests. For the humified sample, SM2C-A3-1C, the pore pressure develops stronger and increases more rapidly at $\gamma_c = 3\%$ than found for the non-to-moderately humified sample, SM2C-B1-2C. Decay in r_u is found for $\gamma_c > 10\%$. The behavior found for the humified sample, SM2C-A3-1C, as shown in Fig. 19(e), corresponds to the behavior found for test SB4A-A2-1C, Fig. 19(d), which is also classified as humified and is equivalent to the differences observed between the humified and non-to-moderately humified specimens in Fig. 16. This comparison indicates that the degree of humification has an influence on the pore pressure development during cyclic testing, which might be explained by the fiber matrix that is present in the non-to-moderately humified material and resistant to compaction during shear. For the humified material the fibers are absent or in strong decay, which reduces the contribution of the fibers to peat behavior.

Resonant Column Testing

This study uses two different test setups for resonant column testing. The first device applied shear strain increments from 0.001% to 0.1%. This equipment was originally built for testing granular materials, with samples being free to rotate at the top and bottom as a free-free resonant column. Sinusoidal rotations are applied at the top using two minishakers mounted on the top cap. To test soft peat specimens, a newly designed, lightweight top cap with actuators (see Fig. 20) was designed and constructed specially for this study. The weight of the top cap and actuators was 5 kg. Before testing, the polar mass moment of inertia of the improved system was determined. The device was then calibrated and validated for shear stiffness and damping ratio using aluminium samples. To prevent slippage between the actuator and the specimen, pins and wings were added to the top cap. The diameter of specimens tested in this device was trimmed to 80 mm. The results are shown as the diamond-shaped points in Figs. 21–23 and 25.

The shear modulus G is found by

$$G = \left(\frac{2\pi f_r}{a}\right)^2 \rho, \quad a\tan(a) - \frac{J^2}{J_0 J_L}\frac{\tan(a)}{a} = \frac{J}{J_0} + \frac{J}{J_L}, \quad a = \frac{\omega L}{v_s} \tag{9}$$

Downloaded from ascelibrary.org by Technische Universiteit Delft on 05/13/20. Copyright ASCE. For personal use only; all rights reserved.

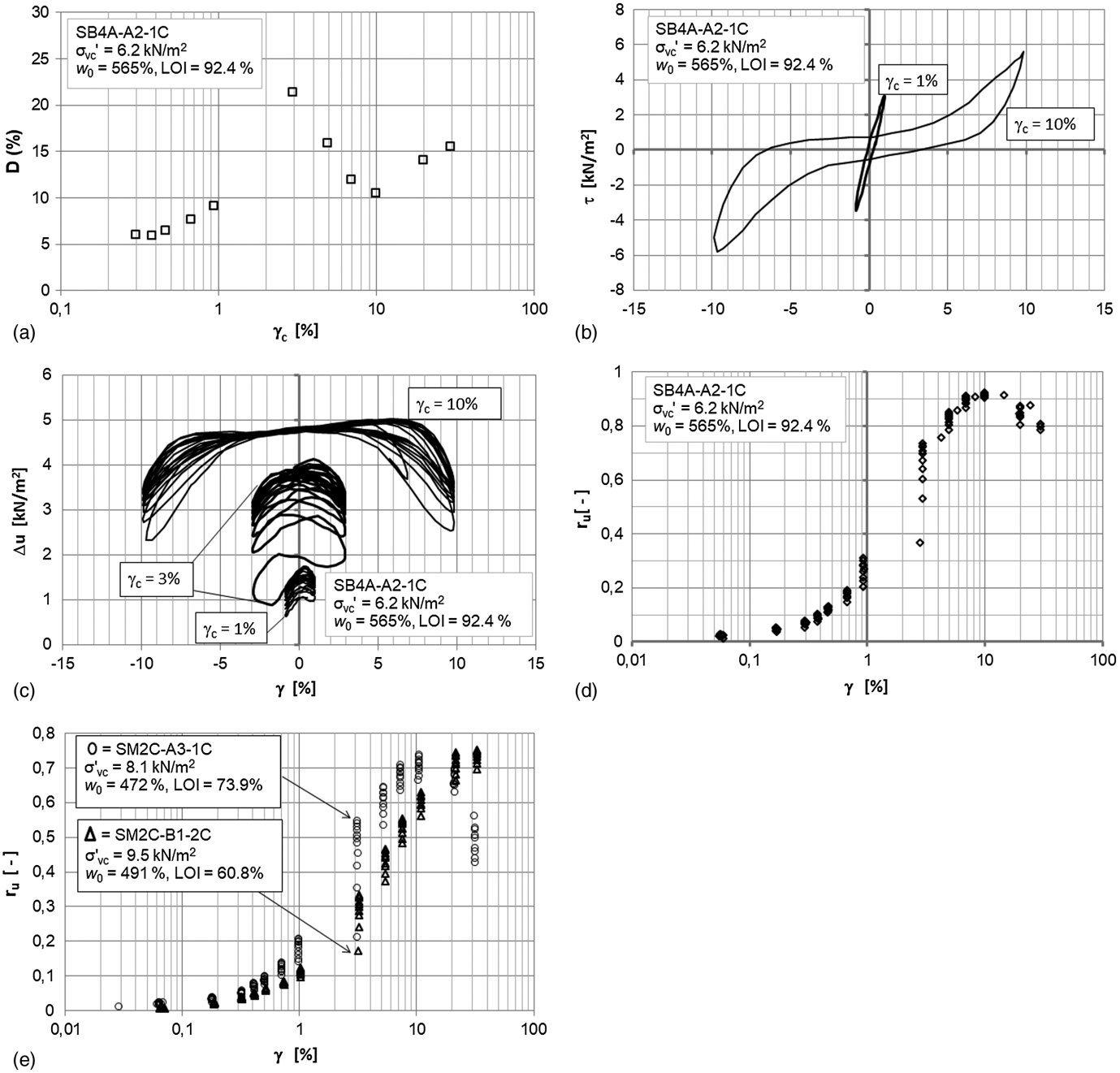

Fig. 19. Details of cyclic DSS test on sample SB4A-A2-1C: (a) damping curve; (b) stress–strain $\tau - \gamma$ cycles at $\gamma_c = 1\%$ and 10%; (c) excess pore pressure development for $\gamma_c = 1\%$, 3%, and 10%; (d) r_u development; and (e) r_u development for both Schildmeer tests; D = damping, τ = shear stress, γ = shear strain, and r_u = excess pore pressure ratio.

where ω = rotational frequency; v_s = the wave velocity; J_0 and J_L = the polar mass moment of inertia of the top and bottom parts of the resonant column; J = the polar mass moment of inertia of the sample; ρ = the density of the sample; f_r = the resonant frequency; and L = the specimen height.

The half-power bandwidth method (Richart et al. 1970; Stokoe et al. 1999; Goudarzy 2015) is used to determine damping D:

$$D = \frac{f_2 - f_1}{2f_r}(\times 100\%) \tag{10}$$

where f_1 and f_2 represent the frequencies at which $\gamma = \sqrt{2} \times \gamma_{\text{peak}}/2$, with γ_{peak} representing the shear strain at $f = f_r$.

The second device was a Hardin oscillator resonant column device, a fixed-free configuration with the oscillator mounted at the top. The results are shown as circles in Figs. 21–23 and 25. The applied shear strain increments ranged between 0.0001% and 0.1%. In this device, the weight of the top cap was counterbalanced by a dead weight so that the weight of the top cap did not apply a vertical force on the sample. The diameter of the specimens tested in this device was trimmed to 54 mm. Pins were used in the top cap and pedestal to prevent slippage.

ASTM D4015 (ASTM 2015) was followed to assess G and D during tests with the second device, with D being determined on the basis of steady state vibration.

J. Geotech. Geoenviron. Eng., 2020, 146(7): 04020049

Downloaded from ascelibrary.org by Technische Universiteit Delft on 05/13/20. Copyright ASCE. For personal use only; all rights reserved.

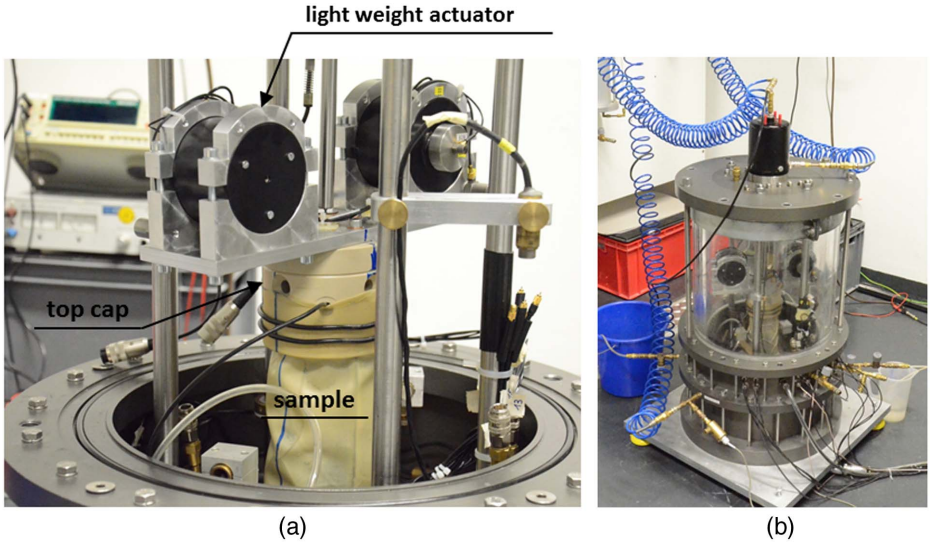

Fig. 20. Photo of RC equipment: (a) lightweight actuator mounted on sample; and (b) complete test setup.

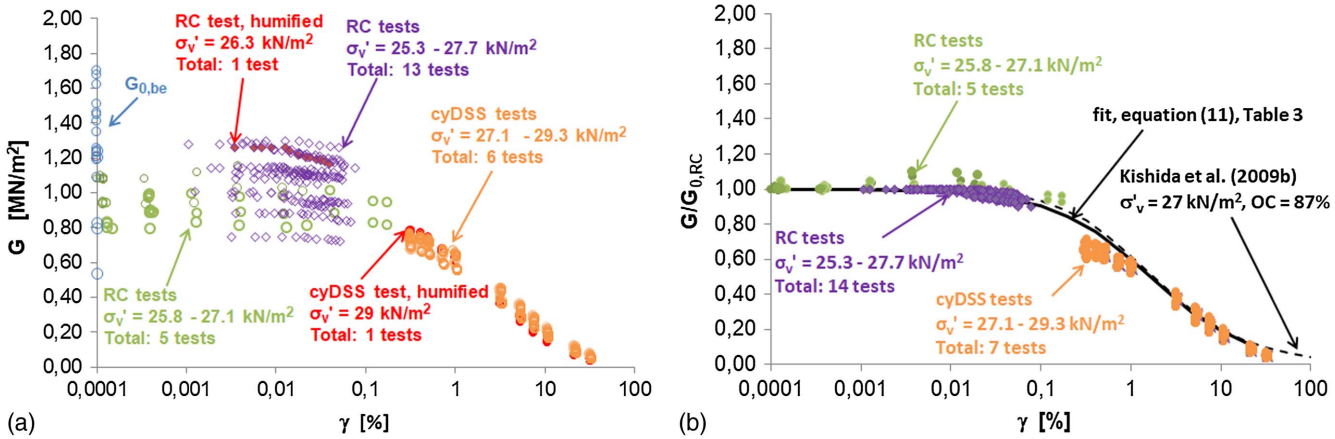

Fig. 21. Shear modulus degradation curve for Nieuwolda location: (a) measured data; and (b) data normalized by $G_{0,RC}$ compared to the relation given by Kishida et al. (2009b) and Eq. (11) and Table 3.

Shear Modulus Reduction Curve

The results of the resonant column tests, the bender element tests, and the cyDSS tests are combined to construct a shear modulus degradation curve. Figs. 21–23 show the results for the three different sample sites.

The $G_{0,RC}$ value was adopted as the largest measured shear modulus during RC testing, typically at shear strains of $\gamma < 0.003\%$, for the normalization of the data. The cyDSS data were normalized using the $G_{0,RC}$ values found from the RC tested specimen from the same sample. The test results indicate a remarkably good match between the different testing techniques. In Figs. 21(a)–23(a), the test results for humified material are shown as the closed dots, while the test results for non-to-moderately humified material are shown as open circles. The range of cyDSS test results is small, and the results for the humified material do not differ significantly from the results for the non-to-moderately humified material. Furthermore, normalization using $G_{0,RC}$ in the right graphs in Figs. 21–23 produces a consistent shear modulus reduction curve with no difference between the humified material and the non-to-moderately humified material.

For reference purposes, the small-strain stiffness $G_{0,be}$ obtained with bender element testing has been plotted on the left of Figs. 21–23. Including all the resonant column data gives $G_{0,RC,ave} = 830$ kN/m^2 and $COV = 0.28$ for $\sigma'_v = 7.6$–13.3 kN/m^2 and $G_{0,RC,\text{ave}} = 1{,}030$ kN/m^2 and $COV = 0.14$ for $\sigma'_v = 25.3$–27.7 kN/m^2.

Fig. 24 shows a direct comparison of the values for $G_{0,be}$ and $G_{0,RC}$ obtained for the same specimens. The graph shows approximately $G_{0,be} = 1.3 \times G_{0,RC}$. This is slightly larger than the 20% difference observed by Wehling et al. (2003) in a comparison of the values for $G_{0,be}$ and $G_{0,RC}$ from cyclic triaxial testing. The differences in $G_{0,RC}$ and $G_{0,be}$ are considered to be small given the complex nature of the tested material, and they could be explained by the different measurement techniques. These findings match those of Dyvik and Madshus (1985), who found a good match between $G_{0,RC}$ and $G_{0,be}$ for different clays consolidated at different confining stress levels, resulting in a G_0 range of 10–150 MN/m^2.

Figs. 21–23 show that shear modulus reduction curves for the Groningen peat samples are almost linear and horizontal up to

J. Geotech. Geoenviron. Eng., 2020, 146(7): 04020049

Downloaded from ascelibrary.org by Technische Universiteit Delft on 05/13/20. Copyright ASCE. For personal use only; all rights reserved.

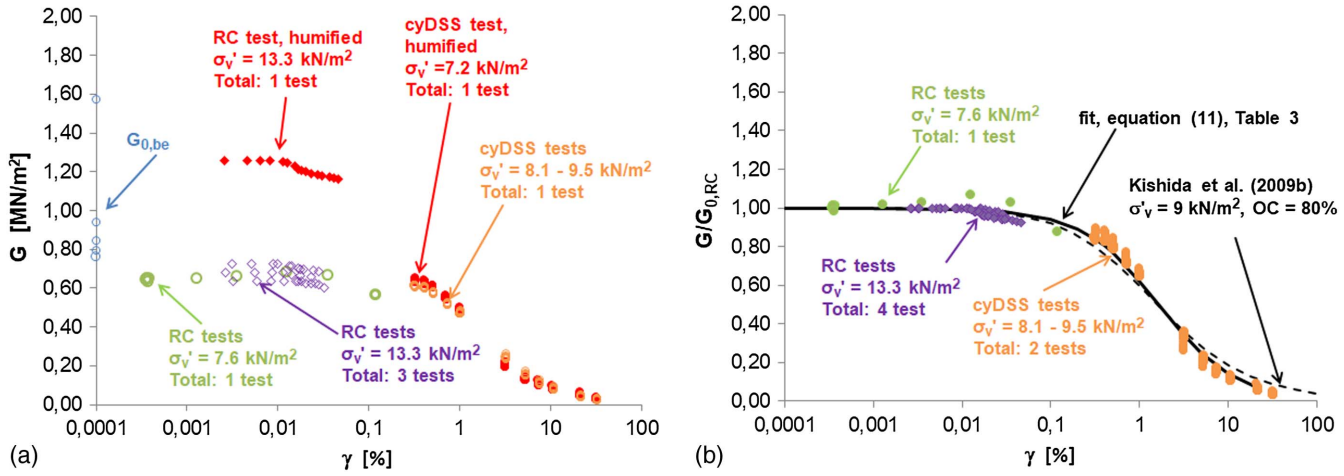

Fig. 22. Shear modulus degradation curve for Schildmeer location: (a) measured data; and (b) data normalized by $G_{0,RC}$ compared to the relation given by Kishida et al. (2009b) and Eq. (11) and Table 3.

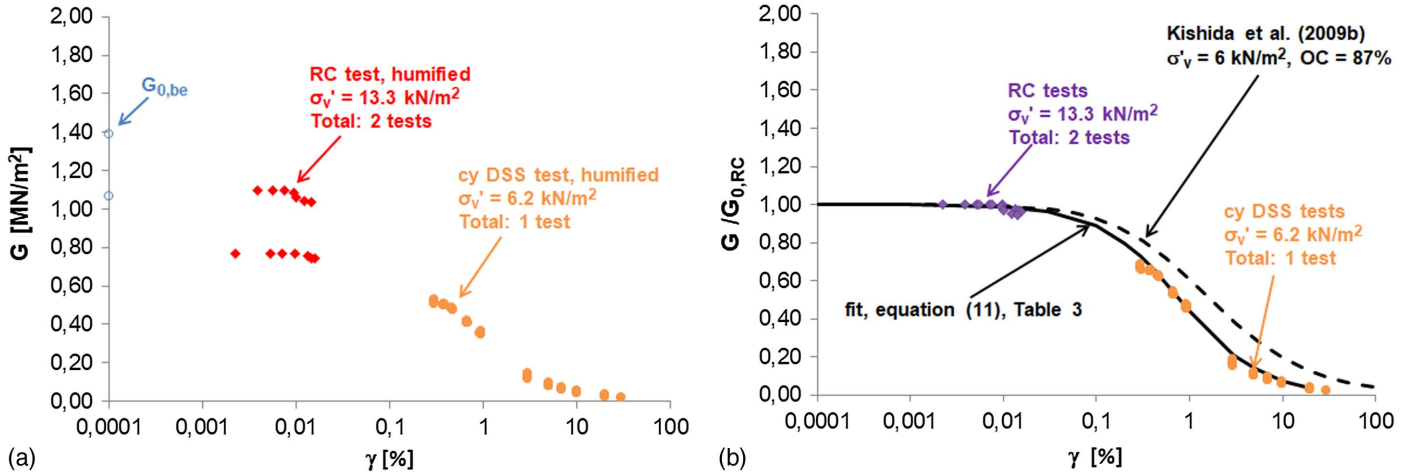

Fig. 23. Shear modulus degradation curve for Siddeburen location: (a) measured data; and (b) data normalized by $G_{0,RC}$ compared to the relation given by Kishida et al. (2009b) and Eq. (11) and Table 3.

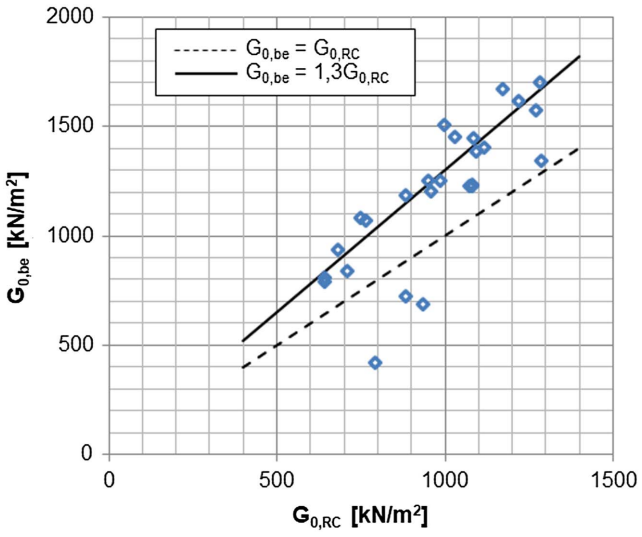

Fig. 24. Comparison between $G_{0,be}$ and $G_{0,RC}$ for all RC tests.

approximately $\gamma = 0.01\%$. The shear modulus values fall progressively with increasing strain levels. The data was fitted using Eq. (11) [(Kondner and Zelasko 1963), modified by Matasovic and Vucetic (1993)]

$$\frac{G}{G_0} = \frac{1}{1 + \beta\left(\frac{\gamma}{\gamma_{ref}}\right)^{\alpha}} \tag{11}$$

where α and β are fit parameters and γ_{ref} represents a reference shear strain. In accordance with Stokoe et al. (1999), γ_{ref} represents the strain level at which $G/G_0 = 0.5$, implying $\beta = 1$. This is valid if experimental data encompassing $G/G_0 = 0.5$ is available. Due to the stepwise increase of γ in the cyclic DSS tests, γ_{ref} is not measured exactly because it is located between two steps. Consequently, γ_{ref} is estimated from the adjacent steps in which G/G_0 drops below 0.5. The value for α is then found by curve fitting. The values obtained for γ_{ref} and α are summarized in Table 3, and the corresponding curves are presented in Figs. 21(b)–23(b).

The Nieuwolda and Schildmeer data lead to approximately the same γ_{ref}, while the Schildmeer data yields a larger α than found

J. Geotech. Geoenviron. Eng., 2020, 146(7): 04020049

Downloaded from ascelibrary.org by Technische Universiteit Delft on 05/13/20. Copyright ASCE. For personal use only; all rights reserved.

Table 3. γ_{ref} for the three sample locations

Location	γ_{ref} (%)	α
Nieuwolda	1.65	0.8
Schildmeer	1.65	1.2
Siddeburen	0.80	1.0

for the Nieuwolda data. In the Siddeburen data, γ_{ref} is lower than in the Nieuwolda and Schildmeer data and the value for α is located between values in Nieuwolda and Schilmeer data.

The effect of the applied stress level on the normalized shear modulus reduction curve is not clear. Although the specimens from the Siddeburen and Schildmeer locations were tested at equivalent stress levels, a clear difference was found for γ_{ref}. In the specimens from Nieuwolda, which were tested at the highest stress level, γ_{ref} was approximately the same as in the specimens from the Schildmeer location. It should be noted that the samples were consolidated at field stress level and that all samples were therefore tested for overconsolidated conditions.

The apparently minor impact of applied stress corresponds to the findings presented by Kishida et al. (2009a), who found that in strong organic material, $OC > 65\%$, the effect of the consolidation stress is less apparent than in nonorganic soils.

Damping Curve

Fig. 25 shows the damping curves obtained from the resonant column and the cyDSS tests for each of the sample locations. There is more scatter in the damping curves than in the shear modulus reduction curves. The humified specimens at the Schildmeer location [Fig. 25(b)] and the Siddeburen location [Fig. 25(c)] both show a discontinuity for $\gamma_c = 3\%$, which was further investigated by Fig. 19.

The damping behavior in the two types of resonant column testing is different at low shear strain amplitudes. The differences are most apparent in the Nieuwolda case. It should be noted that, in addition to there being differences in the testing equipment, the damping ratio was also evaluated differently, as explained in the "Resonant Column Testing" section. The measurements and analysis of the data have been carefully checked. Both types of equipment and corresponding analysis of measurement data are commonly used and valid. The cause of the different outcome forms a topic of further research. An explanation might be found in the nature of the material. Peats are soft materials, therefore the resonant frequency and the applied amplitude for vibration to generate a given shear strain is much less than the resonant frequency and the adopted amplitude for the conventional soils, e.g., sands, especially in the experiment using the adopted resonant column devices. This will significantly increase the effect of noise and near-field effects on the measured damping ratio. For increased applied shear strain level, the effect of noise and near-field effects will be relatively less pronounced, and the accuracy of the estimated damping will increase [see also Stokoe et al. (1999) for more details on this issue].

The high initial damping values $D_{\min}$ reaching up to 15%, as shown in Fig. 25(a), might be due to the effect of noise and near-field effects rather than material response. Instead, $D_{\min}$ is estimated using the first method, diamonds in Fig. 25, which yields $D_{\min} = 4.8\%$ at the Nieuwolda location, 6.5% at the Schildmeer location, and 8.5% at Siddeburen. It should be noted that the data is scattered and an exact value is difficult to obtain. The data is compared to the regression model given by Kishida et al. (2009b), which suggest a lower initial damping ratio $D_{\min}$ than found in the tests.

Among others, Wehling et al. (2003) have found a decreasing trend in damping ratio with increasing consolidation stress. The data follows this trend: the $D_{\min}$ value for the Schildmeer and Siddeburen locations is larger than for the Nieuwolda location, where tests were conducted at higher stress levels. Fig. 25 also identifies the tests on humified material. The damping behavior of the humified material does not seem to differ from the damping behavior of the non-to-moderately humified material.

Figs. 25(a and b) provide the general trend by the dotted line. This general trend is drawn manually as best fit through the data points. The general trends for the Nieuwolda and Schildmeer specimens are compared with the literature data in Fig. 26. Because only a limited number of tests were conducted at the Siddeburen location, those results have been omitted in Fig. 26 to enhance clarity. The applied consolidation stress level and the organic content have been identified as the dominant factors that affect the dynamic behavior of organic soils (Kishida et al. 2009a; Kramer 2000). A comparison of the data from samples subjected to different testing modes (triaxial, resonant column, and torsional shear) did not show that the shearing direction had a significant effect on the dynamic parameters G, G/G_0, or D (Kishida et al. 2009a).

Fig. 26 compares the Nieuwolda and Schildmeer data with three test series discussed in the literature. The first data series is from Wehling et al. (2003). The second series is from Boulanger et al. (1998). The third series considers the organic, highly decomposed soil from the Montezuma Slough area in California (Kishida et al. 2009a). Details of these test series are shown in Table 1.

Fig. 26 shows that consolidation stress has an effect on damping ratio values at low stress levels. As shown by the damping ratio data from Boulanger et al. (1998), those values are not affected by consolidation stress in the range from 66 to 200 kN/m^2. The effect of consolidation stress on the damping data for the Groningen peat samples is evident, at least for the range of stresses considered. The D values where $\sigma'_{vc} = 5.5$–13.3 kN/m^2 tend to be larger than those for samples where $\sigma'_{vc} = 25.3$–29.3 kN/m^2.

Fig. 26 also shows that the damping ratio curve for the Nieuwolda and Schildmeer locations concurs with the data for organic soils in the literature. However, at shear strain levels above 0.01%, the damping ratio found for the Nieuwolda site seems low by comparison with the published data for similar stress levels. The data from the Schildmeer location are also below the damping curve found by Wehling et al. (2003) for low stress levels. This behavior could be attributed to the fact that the organic content of the Groningen peat samples tested, which ranged from 70% to 95%, was higher than in the other tests. Kishida et al. (2009a) reported for peat samples from Sacramento–San Joaquin delta, California, that the damping ratio tends to decrease, given similar consolidation stress levels, for increasing OC values. The results presented above seem to follow this trend.

Conclusions

A series of laboratory tests was conducted to establish the dynamic parameters of the Groningen peat deposit. The organic content of the samples tested is higher than reported for the majority of tests in the literature on the dynamic behavior of organic soils. In general, the test results for peat were within the range of published data for organic soils. Shear wave velocities were found by bender element testing in the range of 20.3–40.6 m/s and corresponding small-strain shear moduli in the range of 421–1,704 kN/m^2.

Downloaded from ascelibrary.org by Technische Universiteit Delft on 05/13/20. Copyright ASCE. For personal use only; all rights reserved.

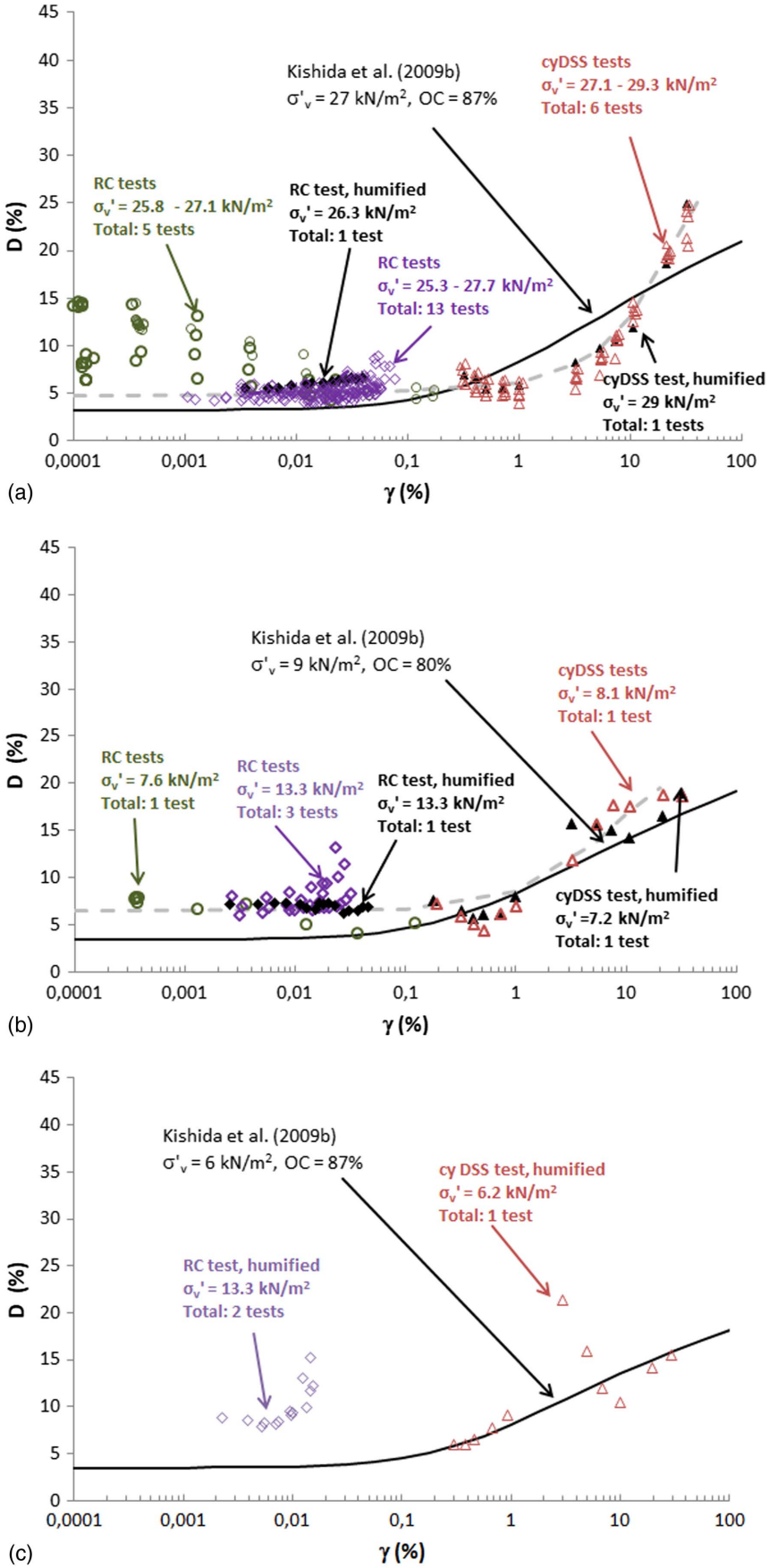

Fig. 25. Damping curves for (a) Nieuwolda; (b) Schildmeer; and (c) Siddeburen; the grey dotted lines in (a and b) represent a general trend line, drawn manually through the data.

J. Geotech. Geoenviron. Eng., 2020, 146(7): 04020049

Downloaded from ascelibrary.org by Technische Universiteit Delft on 05/13/20. Copyright ASCE. For personal use only; all rights reserved.

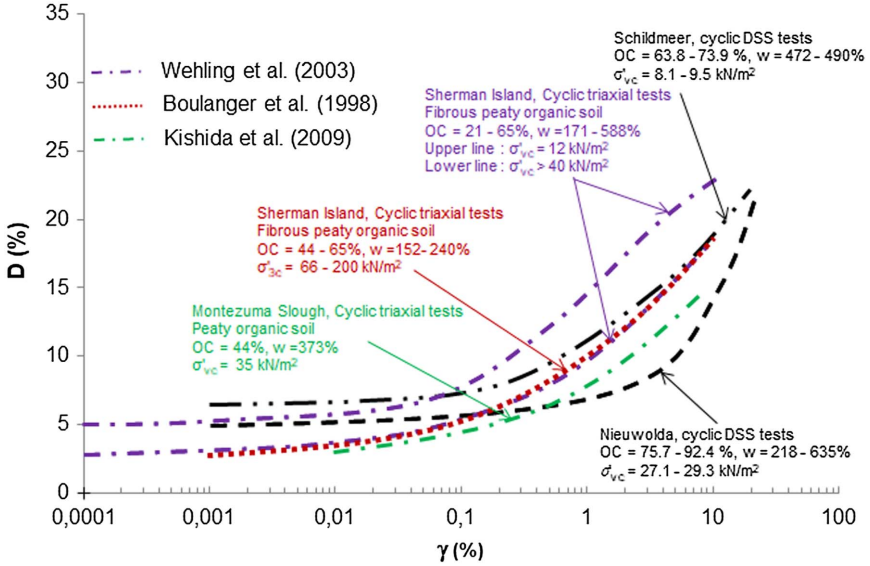

Fig. 26. Comparison of general trends in damping curve for Nieuwolda and Schildmeer tests (black line) with literature data.

The shear modulus reduction curves obtained with the different testing techniques match each other well and comply with the regression model given by Kishida et al. (2009b). There were experimental difficulties affecting the assessment of the damping curve. However, the general trends in the damping curves obtained concurred with the available literature.

Detailed analysis of pore pressure development during cyclic shearing indicates two phenomena. The first is a gradual pore pressure buildup during the successive cycles, which shows a tendency for compaction. The second is a drop in pore pressure when reaching maximum displacement in each cycle, which corresponds to dilative behavior. For small γ_c, the tendency for compaction dominates and a gradual buildup of pore pressure in the successive cycles is found. For large γ_c the pore pressure buildup during the successive cycles are negligible; however, a strong, reversible reduction in pore pressure is found at maximum displacement for each cycle. For the humified samples, the pore pressure buildup during the early stages of the test is stronger than for the non-to-moderately humified material. This might be explained by the absence of a strong fiber matrix in the humified samples that could resist shearing compaction.

A rapid increase in pore pressure buildup is found in all the tests at $\gamma_c = 3\%$. For the humified samples, however, this effect is stronger, as shown by Fig. 19(d), with r_u increasing from 0.37 to 0.72, which corresponds to a discontinuity in the damping curve for specimens tested at low stress level.

In contrast with the literature, the differences in the organic content of the Groningen peat, $OC = 70\%–95\%$, had hardly any impact on the dynamic parameters. It should be noted that the range of the organic content of the Groningen peat deposit is relatively narrow. It is possible that there is a threshold value below which OC has a significant effect on dynamic parameters and that the OC for the tested peat is above this threshold value.

Eq. (4) (Wehling et al. 2003) is suitable for predicting the normalized small-strain shear modulus using vertical effective stress and OCR when using the parameters n and m from Kishida et al. (2009b) [Eq. (6)]. However, the predictions for parameter A given by Wehling et al. (2003) or Kishida et al. (2006) do not fit the data. Instead, a considerable lower value, $A = 38.65$, reproduces the data best.

An attempt was made to study the influence of the fiber matrix by classifying the samples as humified and non-to-moderately humified material. The appendix shows that the differences in water content, loss on ignition, void ratio, and dry and solid density between the two groups are statistically significant. Besides a difference in observed excess pore pressure development, discussed previously, no significant difference in shear modulus reduction curve [Figs. 21(a)–23(b)] and damping curve [Figs. 25(a–c)] are found. It should be noted that, due to the limited thickness of patches of humified material, only a small number of humified samples could be taken.

Appendix. Verification of Visual Classification in Humified and Non-humified Material

The tested material was classified visually as humified and non-to-moderately humified. A difference in the degree of humification should be reflected by a difference in the classification parameters. F- and T-tests were applied to test the statistical significance of the differences observed in the classification parameters. An explanation of the F- and T-tests is given by Kanji (2006). The T-test poses the hypothesis that the mean value of two populations X and Y, here the humified and non-to-moderately humified material, are equal given random selections from each population. In order to apply the T-test, the F-test should be conducted first, which tests the variance of both populations. If the F-tests fails, the T-test is replaced by the more complex Welch test.

A total of 76 test results were assessed: 63 results on specimens classified as non-to-moderately humified and 13 test results on humified material. Table 4 gives the mean and the 5% and 95% probability of exceedance values. In the humified material, the difference between the lower and upper values for each of the classification parameters is larger, indicating greater variability in humified material.

Table 5 gives the results for the T-test by which the hypothesis that the humified and non-to-moderately humified material have the same mean value for the different classification parameters is tested. Table 5 provides the value for the testing parameter T. The testing parameter T has a student-t distribution. The hypothesis is excepted with 90% confidence level when $t_m^{0.05} < T < t_m^{0.95}$,

Downloaded from ascelibrary.org by Technische Universiteit Delft on 05/13/20. Copyright ASCE. For personal use only; all rights reserved.

Table 4. Summary of classification parameters for humified and non-to-moderately humified peat samples; the presented ranges refer to the 95% upper and lower boundary values

Parameter	Symbol	Unit	Humified	Non-to-moderately humified
Bulk density	ρ	Mg/m^3	1.00 ± 0.0294	0.99 ± 0.0127
Dry density	ρ_{dry}	Mg/m^3	0.18 ± 0.0279	0.15 ± 0.0046
Solid density	ρ_s	Mg/m^3	1.57 ± 0.0776	1.51 ± 0.0144
Natural water content	w_0	%	485 ± 46.75	556 ± 17.29
Loss on ignition	LOI	%	81.85 ± 6.22	86.14 ± 1.33
Void ratio	e_0	—	8.16 ± 0.776	9.01 ± 0.288

Table 5. Results of T-test, with $t_m^{0.05} = -1.67$ and $t_m^{0.95} = 1.67$

Parameters	ρ	ρ_{dry}	ρ_s	w_0	LOI	e_0
T	0.51	2.77	2.06	−2.75	−1.83	−1.99
$P(T < t; H_0)$	0.695	0.997	0.979	0.004	0.036	0.025
Conclusion	Accepted	Rejected	Rejected	Rejected	Rejected	Rejected

which is equivalent to the probability that $T < t$ given the stated hypothesis H_0, $P(T < t; H_0)$, which is also given in Table 5. Except for ρ, the hypothesis H_0 is rejected for the different parameters, meaning that the difference in the *mean* value with the different parameters for the humified and non-to-moderately humified material is statistically significant. The outcome of the statistical tests supports the visually made classification.

Acknowledgments

The authors would like to express their gratitude to Professor Tom Schanz for his significant contribution to this work. Professor Schanz passed away during the drafting of this paper. The authors would also like to thank NAM for financing this research. Thanks are also due to Sieb de Vries and Peter Vos for providing the geological background and classification of the tested material. Furthermore, the authors acknowledge the valuable comments given by the reviewers.

Notation

The following symbols are used in this paper:

A = parameter used in Eqs. (4) and (5);
C = parameter in Eq. (1);
C_c, CR = compression index;
C_α = creep index;
D = damping ratio;
D_{min} = initial damping ratio, damping ratio at low shear strain amplitudes;
e_0 = initial void ratio;
f_r = resonant frequency;
f_1, f_2 = frequencies at which $\gamma = \sqrt{2} \times \gamma_{peak}/2$;
G, G_N = shear modulus, shear modulus Nth cycle;
G_0, $G_{0,be,RC}$ = small-strain shear modulus, small-strain shear modulus obtained by bender element testing and resonant column testing, respectively;
J, J_0, J_L = polar mass moment of inertia of the sample, the bottom or top part, respectively;
L = specimen height;
N = number of cycles;
n, m = exponent used in Eq. (4);
p' = mean effective stress;
p_a = atmospheric pressure;
q = deviator stress;
r_u = excess pore pressure ratio;
S = undrained shear strength ratio;
s_u = undrained shear strength;
t = degradation parameter, Eq. (7);
v_s = shear wave velocity;
W_D, W_S = energy dissipated per cycle, energy stored per cycle;
w, w_0 = water content, initial water content prior to laboratory testing;
α, β = parameters used in Eq. (11);
δ = degradation index, Eq. (7);
γ, γ_c = shear strain; target shear strain in cyclic DSS testing;
γ_{peak} = shear strain at $f = f_r$;
γ_{ref} = reference shear strain, shear strain reached at $G/G_0 = 0.5$;
Δu = pore pressure, excess pore pressure in cyclic DSS testing;
μ = strength gain factor, Eq. (2);
ρ, ρ_{dry}, ρ_s = bulk density, dry bulk density, solid density;
σ'_v = vertical effective stress;
σ'_{vc} = vertical consolidation stress, used to describe test conditions;
σ'_{vy} = yield stress, used for field conditions;
τ, τ_{max} = shear stress, maximum shear stress;
τ_{static} = static shear stress; and
ω = rotational frequency.

Supplemental Data

Supplemental data is available online in the ASCE Library (www.ascelibrary.org). The files contain an overview of the classification parameters for all tested specimens and the recorded measurements data of the cyDSS tests.

References

APS (Antriebs-, Prüf- und Steuertechnik GmbH). 2019. "Product specifications direct simple shear device." Accessed May 5, 2019. https://www.wille-Geotechnik.com/en/Simple_Shear_Systems.html.

ASTM. 2015. *Standard test methods for modulus and damping of soils by fixed-base resonant column devices.* ASTM D4015. West Conshohocken, PA: ASTM.

Azzouz, A. S., R. J. Krizek, and R. B. Corotis. 1976. "Regression analysis of soil compressibility." *Soils Found.* 16 (2): 19–29. https://doi.org/10.3208/sandf1972.16.2_19.

Boulanger, R. W., R. Arulnathan, L. F. Harder, R. A. Torres, and M. W. Driller. 1998. "Dynamic properties of Sherman Island peat." *J. Geotech. Geoenviron. Eng.* 24 (1): 12–20. https://doi.org/10.1061/(ASCE)1090-0241(1998)124:1(12).

Cappa, R., S. J. Brandenberg, and A. Lemnitzer. 2017. "Strains and pore pressures generated during cyclic loading of embankments on organic soil." *J. Geotech. Geoenviron. Eng.* 143 (9): 04017069. https://doi.org/10.1061/(ASCE)GT.1943-5606.0001721.

Cola, S., and G. Cortellazzo. 2005. "The shear strength behaviour of two peaty soils." *Geotech. Geol. Eng.* 23: 679–695. https://doi.org/10.1007/s10706-004-9223-9.

CROW (Centrum voor Regelgeving en Onderzoek Grond-, Water-, en Wegenbouw). 2015. *Standaard RAW bepalingen, proef 28.* [In Dutch.] Ede, Netherlands: CROW.

Downloaded from ascelibrary.org by Technische Universiteit Delft on 05/13/20. Copyright ASCE. For personal use only; all rights reserved.

De Groot, M. B., M. D. Bolton, P. Foray, P. Meijers, A. C. Palmer, R. Sandven, A. Sawicki, and T. C. Teh. 2006. "Physics of liquefaction phenomena around marine structures." *J. Waterway, Port, Coastal, Ocean Eng.* 132 (4): 227–243. https://doi.org/10.1061/(ASCE)0733-950X(2006)132:4(227).

Den Haan, E. J. 2014. "Modelling peat with an anisotropic time-dependent model for clay." In *Numerical methods in geotechnical engineering*, edited by M. A. Hicks, R. B. J. Brinkgreve, and A. Rohe. London: Taylor & Francis Group.

Den Haan, E. J., and G. A. M. Kruse. 2007. "Characterisation and engineering properties of Dutch peats." In *Characterisation and engineering properties of natural soils*, edited by T. S. Tan, K. K. Phoon, and D. W. Hight. London: Taylor & Francis Group.

Dyvik, R., T. Berre, S. Lacasse, and B. Raadim. 1987. "Comparison of truly undrained and constant volume direct simple shear tests." *Géotechnique* 37 (1): 3–10. https://doi.org/10.1680/geot.1987.37.1.3.

Dyvik, R., and C. Madshus. 1985. "Lab measurements of Gmax using bender elements." In *ASCE annual convention, Advances in the art of testing soils under cyclic conditions*, edited by V. K. Khosla. Reston, VA: ASCE.

Goudarzy, M. 2015. "Micro and macro mechanical assessment of small and intermediate strain properties of granular material." Ph.D. thesis, Foundation Engineering, Soil and Rock Mechanics, Ruhr-Universität Bochum.

Hobbs, N. B. 1986. "Mire morphology and the properties and behaviour of some British and foreign peats." *Q. J. Eng. Geol.* 19: 7–80. https://doi.org/10.1144/GSL.QJEG.1986.019.01.02.

Idriss, I. M., and R. W. Boulanger. 2008. *Soil liquefaction during earthquakes*. Berkeley, CA: Earthquake Engineering Institute.

Idriss, I. M., R. Dobry, and R. D. Singh. 1978. "Nonlinear behaviour of soft clays during cyclic loading." *J. Geotech. Eng. Div. Am. Soc. Civ. Eng.* 104 (12): 1427–1447.

ISO. 2015. *Geotechnical investigation and testing—Laboratory testing of soil. Part 3: Determination of particle density.* ISO 17892-3. Geneva: ISO.

Kallioglou, P., T. Tika, G. Koninis, and S. Papadopoulos, and K. Pitilakis. 2008. "Shear modulus and damping ratio of organic soils." *Geotech. Geol. Eng.* 27 (2): 217. https://doi.org/10.1007/s10706-008-9224-1.

Kanji, G. P. 2006. *100 statistical tests*. 3rd ed. London: SAGE Publications.

Kishida, T., R. W. Boulanger, N. A. Abrahamson, T. M. Wehling, and M. W. Driller. 2009a. "Regression models for dynamic properties of highly organic soils." *J. Geotech. Geoenviron. Eng.* 135 (4): 533–543. https://doi.org/10.1061/(ASCE)1090-0241(2009)135:4(533).

Kishida, T., R. W. Boulanger, T. M. Wehling, and M. W. Driller. 2006. "Variation of small strain stiffness for peat and organic soil." In *Proc., 8th US National Conf. on Earthquake Engineering*. Oakland, CA: Earthquake Engineering Research Institute.

Kishida, T., T. M. Wehling, R. W. Boulanger, M. W. Driller, and K. H. Stokoe, II. 2009b. "Dynamic properties of highly organic soils from Montezuma Slough and Clifton Court." *J. Geotech. Geoenviron. Eng.* 135 (4): 525–532. https://doi.org/10.1061/(ASCE)1090-0241(2009)135:4(525).

Kondner, R. L., and J. S. Zelasko. 1963. "Hyperbolic stress-strain formulation of sands." In *Proc., Second Pan American Conf. on Soil Mechanics and Foundation Engineering*, 289–324. Sao Paulo, Brazil: Associação Brasileira de Mecânica dos Solos.

Kramer, S. L. 1996. *Dynamic response of peat*. Rep. No. WA-RD 412.2. Olympia, WA: Washington State DOT.

Kramer, S. L. 2000. "Dynamic response of mercer slough peat." *J. Geotech. Geoenviron. Eng.* 126 (6): 504–510. https://doi.org/10.1061/(ASCE)1090-0241(2000)126:6(504).

Kruiver, P. P., et al. 2017. "An integrated shear-wave velocity model for the Groningen gas field, The Netherlands." *Bull. Earthquake Eng.* 15 (9): 3555–3580. https://doi.org/10.1007/s10518-017-0105-y.

Ladd, C. C., and R. Foot. 1974. "New design procedure for stability of soft clays." *J. Geotech. Eng. Div.* 100 (GT7): 763–786.

Landva, A. O. 2007. "Characterization of Escuminac peat and construction on peatland." In *Characterisation and engineering properties of natural soils*, edited by T. S. Tan, K. K. Phoon, and D. W. Hight. London: Taylor & Francis Group.

Matasovic, N., and M. Vucetic. 1993. "Cyclic characterization of liquefiable sands." *J. Geotech. Geoenviron. Eng.* 119 (11): 1805–1822. https://doi.org/10.1061/(ASCE)0733-9410(1993)119:11(1805).

Mesri, G., and M. Ajlouni. 2007. "Engineering properties of fibrous peats." *J. Geotech. Geoenviron. Eng.* 133 (7): 850–866. https://doi.org/10.1061/(ASCE)1090-0241(2007)133:7(850).

Richart, F. E., J. R. Hall, and R. D. Woods. 1970. *Vibrations of soils and foundations*. Englewood Cliffs, NJ: Prentice-Hall.

Shafiee, A. 2016. "Cyclic and post-cyclic behavior of Sherman Island peat." Ph.D. thesis, Dept. of Civil and Environmental Engineering, Univ. of California, Los Angeles.

Skempton, A. W., and D. J. Petley. 1970. "Ignition loss and other properties of peats and clays from Avonmouth, King's Lynn and Cranberry Moss." *Géotechnique* 20 (4): 343–356. https://doi.org/10.1680/geot.1970.20.4.343.

Stokoe, K. H., II, M. B. Darendeli, R. D. Andrus, and L. T. Brown. 1999. "Dynamic soil properties: Laboratory, field and correlation studies." In *Proc., 2nd Int. Conf. on Earthquake Geotechnical Engineering Conf.*, edited by P. S. Sêco e Pinto. Rotterdam, Netherlands: A.A. Balkema.

Stokoe, K. H., II, and J. C. Santamarina. 2000. "Seismic wave based testing in geotechnical engineering." In *Proc., GeoEng.*, 1490–1536. Lisbon, Portugal: International Society for Rock Mechanics and Rock Engineering.

Tokimatsu, K., and T. Sekiguchi. 2006. "Effects of nonlinear properties of surface soils on strong ground motions recorded in Ojiya during 2004 mid Niigata Prefecture earthquake." *Soils Found.* 46 (6): 765–775. https://doi.org/10.3208/sandf.46.765.

Weerts, H. J. T., P. Cleveringa, F. D. de Lang, and W. E. Westerhoff. 2000. *De lithostratigrafische indeling van Nederland. Formaties uit het tertiair en kwartair* [The lithostratigraphical classification of the Netherlands. The quarternary and tertiary formations]. [In Dutch.] TNO rapport 00-95-A. Utrecht, Netherlands: Nederlands Instituut voor Toegepaste Geowetenschappen TNO.

Wehling, T. M., R. W. Boulanger, R. Arulnathan, L. F. Harder, and M. W. Driller. 2003. "Nonlinear dynamic properties of a fibrous organic soil." *J. Geotech. Geoenviron. Eng.* 129 (10): 929–939. https://doi.org/10.1061/(ASCE)1090-0241(2003)129:10(929).

Wood, D. M. 1990. *Soil behaviour and critical state soil mechanics*. Cambridge, UK: Cambridge University Press.

Wroth, C. P. 1984. "The interpretation of in situ soil tests." *Géotechnique* 34 (4): 449–489. https://doi.org/10.1680/geot.1984.34.4.449.

Yamaguchi, H., Y. Ohira, K. Kogure, and S. Mori. 1985. "Undrained shear characteristics of normally consolidated peat under triaxial compression and extension." *Soils Found.* 25 (3): 1–18. https://doi.org/10.3208/sandf1972.25.3_1.

Zwanenburg, C., and R. J. Jardine. 2015. "Laboratory, in situ and full-scale load tests to assess flood embankment stability on peat." *Géotechnique* 65 (4): 309–326. https://doi.org/10.1680/geot.14.P.257.

Downloaded from ascelibrary.org by Technische Universiteit Delft on 05/13/20. Copyright ASCE. For personal use only; all rights reserved.